CyAbrB2 is a nucleoid-associated protein in *Synechocystis* controlling hydrogenase expression during fermentation

Ryo Kariyazono[a] and Takashi Osanai[a]*

[a] School of Agriculture, Meiji University, 1-1-1 Higashimita, Tama-ku, Kawasaki, Kanagawa 214-8571, Japan

*Corresponding author: Takashi Osanai
Meiji University, 1-1-1 Higashimita, Tama-ku, Kawasaki, Kanagawa 214-8571, Japan
Tel: +81-44-934-7103; Fax: +81-44-934-7103; e-mail: tosanai@meiji.ac.jp

Summary

Cyanobacteria, which are oxygenic photosynthetic bacteria, possess bidirectional hydrogenase enzymes (encoded by *hox* genes) that produce fermentative H_2 under microoxic conditions, in which a *hox* operon is highly expressed. Although certain global transcriptional regulators governing *hox* expression have been identified in the model cyanobacterium *Synechocystis* sp. PCC 6803, their dynamics under different environmental conditions remain unknown. Here, we demonstrated that cyAbrB2, a *hox* operon repressor, binds to the hox promoter under aerobic conditions. Under microoxic conditions, specific binding of cyAbrB2 on *hox* promoter diminishes, allowing the alternative sigma factor SigE to access and activate gene expression. We also revealed that cyAbrB2 binds broadly to AT-rich genome regions and represses gene expression from these binding regions, similar to the behavior of nucleoid-associated proteins (NAPs). We have shown the differential chromatin conformations around *hox* region in presence and absence of cyAbrB2. Based on this analogy to NAPs, we propose that cyAbrB2 mediates the hox promoter's chromosomal conformation, which becomes more relaxed under microoxic conditions, resulting in fermentative gene expression.

Key words:

Cyanobacteria, nucleoid-associated proteins, hydrogenase, *Synechocystis* sp. PCC 6803, transcription

Introduction

Cyanobacteria carry out oxygenic photosynthesis, converting CO_2 to carbohydrates that are stored as glycogen. During nighttime, stored glycogen is catabolized via glycolysis and respiration. However, due to respiration, cyanobacteria sometimes experience microoxic conditions during the night, resulting in the utilization of glycolytic products as electron acceptors to replenish the oxidized cofactors required for glycolysis, a process known as fermentation (Stal and Moezelaar 1997). Cyanobacteria possess multiple fermentation pathways that they coordinate according to the environment since each pathway has different ATP gain, redox balance, and substrate availability. The euryhaline cyanobacterium *Synechococcus* sp. PCC7002, for example, produces lactate, hydrogen, alanine, succinate, and acetate under dark microoxic conditions (McNeely et al. 2010), whereas the freshwater living cyanobacterium *Synechocystis* sp. PCC 6803 (hereafter referred to as *Synechocystis*) produces acetate, lactate, dicarboxylic acids, and hydrogen (Osanai et al. 2015; Stal and Moezelaar 1997). Genetic manipulations on *Synechocystis* have demonstrated that modulating the expression levels of certain enzymes can alter fermentative metabolic flow (Iijima et al. 2016, 2021), providing evidence for the involvement of transcription in regulating the fermentative pathway.

Hydrogen has attracted significant attention among other cyanobacterial products owing to its

potential as a biofuel. Bidirectional hydrogenase is a key enzyme for H_2 production from protons (Carrieri et al. 2011) and is commonly found in cyanobacteria, except for open ocean habitants (Puggioni, Tempel, and Latifi 2016). This enzyme can utilize NADH, reduced ferredoxin, and flavodoxin as substrates (Gutekunst et al. 2014). Cyanobacterial hydrogenase comprises five subunits (HoxEFUHY) containing nickel and Fe-S clusters, with auxiliary proteins (HypABCDEF) assisting the complex assembly (Cassier-Chauvat, Veaudor, and Chauvat 2014). Although hydrogenase can also use excess electrons from the photosynthetic electron transport chain, photosystem II-generated oxygen can inhibit its activity (Appel et al. 2000). Another metal-ion-harboring and O_2-sensitive enzyme, pyruvate-ferredoxin oxidoreductase (PFOR), oxidizes pyruvate to produce acetyl-CoA during fermentation. PFOR works coordinatedly with hydrogenase to reduce ferredoxin, which hydrogenase uses as an electron donor (Artz et al. 2020; Gutekunst et al. 2014). However, because both hydrogenase and PFOR are sensitive to oxygen and require metal ions, excessive or premature production of these enzymes can lead to futile inactive enzymes, suggesting that transcriptional regulation in response to the environment is essential for optimal energy cost performance.

Promoter recognition by RNA polymerases is an essential step in transcriptional regulation. Sigma factors, which are subunits of RNA polymerase, recognize core promoter sequences. Transcription factors can also bind to promoter regions to either suppress or promote transcription by RNA

polymerase. Nucleoid-associated proteins (NAPs), a type of transcription factor, regulate transcription by modulating chromosomal conformation (Hołówka and Zakrzewska-Czerwińska 2020), although cyanobacterial NAPs remain unidentified.

In *Synechosysits*, the coding genes of HoxEFUHY form a single operon (*sll1220–1226*), while PFOR is encoded in the *nifJ* (*sll0741*) gene. Both *hox* and *nifJ* operons are highly expressed under microoxic conditions (Summerfield, Nagarajan, and Sherman 2011). Genetic analysis has revealed that multiple global transcriptional regulators control *hox* and *nifJ* expression. Sigma factor SigE (Sll1689) controls the expression of *hox* and *nifJ* operons (Osanai et al. 2005, 2011), while transcription factor cyAbrB2 (Sll0822) represses them (Dutheil et al. 2012; Leplat et al. 2013). Positive regulators for the *hox* operon include LexA (Sll1626) and cyAbrB1 (Sll0329) (Gutekunst et al. 2005; Oliveira and Lindblad 2005, 2008).

SigE is an alternative sigma factor that controls the expression of genes involved in glycogen catabolism and glycolysis, such as PFOR/*nifJ* and hydrogenase (Osanai et al. 2005). SigE shares a high amino acid sequence homology with the primary sigma factor SigA, which is responsible for transcribing housekeeping and photosynthetic genes (Imamura and Asayama 2009). A ChIP-seq study revealed that, while most SigE-binding sites are the same as SigA, SigE exclusively occupies the promoters of glycogen catabolism and glycolysis (Kariyazono and Osanai 2022).

CyAbrB2 and its homolog cyAbrB1 are transcription factors highly conserved in cyanobacteria.

CyAbrB2 regulates the expression of several genes involved in carbon metabolism, nitrogen metabolism, and cell division (Ishii and Hihara 2008; Leplat et al. 2013; Lieman-Hurwitz et al. 2009). CyAbrB2 binds to the *hox* promoter *in vitro* and represses its expression *in vivo* (Dutheil et al. 2012). CyAbrB1, an essential gene, physically interacts with the CyAbrB2 protein (Yamauchi et al. 2011) and binds the *hox* promotor region *in vitro* to promote its expression (Oliveira and Lindblad 2008).

Upon entry into microoxic conditions, SigE, LexA, CyAbrB2, and CyAbrB1 are expected to bind dynamically or dissociate from the *hox* promoter region, although this mechanism remains unclear. To explore this, we conducted a time-course analysis of the transcriptome and ChIP-seq of SigE and CyAbrB2. The *hox* and *nifJ* operons exhibited transient upregulation, behaving distinctly from other microoxic upregulated genes. SigE and cyAbrB2 predominantly controlled transiently upregulated genes. CyAbrB2 was found to bind to long tracts of AT-rich regions in the genome and repress expression from its binding regions under aerobic conditions. The behavior of CyAbrB2 resembled that of NAPs, with binding regions including the *hox* and *nifJ* promoter and gene bodies. Interestingly, CyAbrB2 binding to the *hox* and *nifJ* promoters became less specific under microoxic conditions, while SigE binding to these promoters became prominent. We propose that cyAbrB2 modulates chromosomal conformation like NAPs, allowing access to the SigE-containing RNA polymerase complex.

Results

Transcriptomes on entry to dark microoxic conditions

To understand transcriptional regulation under microoxic conditions, a time-course transcriptome capturing aerobic and microoxic conditions at 1-, 2-, and 4-h timepoints was conducted (Figure 1A). Gene set enrichment analysis revealed that many biological pathways, including photosynthesis and respiration (oxidative phosphorylation), were downregulated under microoxic conditions compared to aerobic conditions (Figure 1B). Upregulated pathways included butanoate metabolism and two-component systems, but the actual cyanobacterial catabolic pathway differed slightly from that described in the KEGG pathway. Within 1 hour of switching from aerobic to anaerobic conditions, the expression levels of 508 genes increased more than 2-fold. Furthermore, genes with increased expression levels were classified into four based on the time-course (Figure 1C). Of the 508 genes, 28 were termed "transiently upregulated genes" due to their decreased expression upon the comparison of 1- and 4-h incubation under microoxic conditions (log2 fold change < -0.5) and 119, which continuously increased between 1- and 4-h incubation under microoxic conditions (log2-fold change > 0.5), were termed "continuously upregulated genes." Mapping the classified genes to central carbon metabolism revealed that *nifJ* encoding PFOR and *hox* operon encoding a bidirectional hydrogenase complex were transiently upregulated (Figure 1D and Table 1). We

verified the transient expression of *hoxF*, *hoxH* and *nifJ* by RTqPCR (Figure S1).

SigE and CyAbrB2 control the expression of transiently upregulated genes

The functional correlation between hydrogenase and PFOR, which are respectively encoded by the *hox* operon and *nifJ*, suggests that transient upregulation has physiological significance. We focused on transiently upregulated genes and attempted to reveal the regulatory mechanism underlying transient upregulation. While SigE promotes expression *hox* and *nifJ*, CyAbrB2 represses them (Dutheil et al. 2012; Leplat et al. 2013; Osanai et al. 2005). We confirmed that the deletion of SigE and cyAbrB2 affected the expression of *hoxF*, *hoxH*, and *nifJ* (Figure S1). Thus, we generated *Synechocystis* mutants with disrupted SigE or CyAbrB2 (Figure S2A) and conducted a time-course transcriptome analysis of the disruptants under aerobic conditions and after 1- and 2-h cultivation in dark microoxic conditions (Figure 2A). The transcriptome data confirmed that both SigE and CyAbrB2 regulated *hox* operon expression (Figure 2B). At each timepoint, we searched for DEGs between mutants and wildtype with a more than 2-fold expression change and a false discovery rate (FDR) less than 0.05. We found that deleting SigE or cyAbrB2 preferentially affected the expression of transiently upregulated genes (Figures 2C and 2D). Interestingly, CyAbrB2 deletion resulted in the upregulation of transient genes under aerobic conditions, in contrast to 1 hour cultivation under microoxic conditions (Figure 2C).

Genome-wide analysis of CyAbrB2, CyAbrB1, and SigE via ChIP-seq

To decipher the regulatory mechanism of transiently upregulated genes, we must first comprehend the fundamental features and functions of these transcriptional regulators. Therefore, we conducted a genome-wide survey of CyAbrB2 and SigE occupation (Figures S2 and S3) and compared it with transcriptome data. Specifically, we generated a *Synechocystis* strain in which CyAbrB2 was epitope-tagged and performed a ChIP-seq assay under aerobic and microoxic conditions (Figures S2B and S2C). SigE-tagged strains previously constructed and analyzed elsewhere were also employed (Kariyazono and Osanai 2022). The primary sigma factor SigA was also analyzed to determine SigE-specific binding. In addition to CyAbrB2, we generated tagged CyAbrB1, the interactor of CyAbrB2 and positive regulator of the *hox* operon.

CyAbrB2 binds to long tracts of the genomic region and suppresses genes in the binding region

The ChIP-seq data from Flag-tagged CyAbrB2 showed that this protein bound to long tracts of the genomic region with lower GC content than the whole genome *Synechocystis* (Figures 3A and 3B). In addition, regions exhibiting lower GC contents showed a greater binding signal of CyAbrB2 (Figure 3C). Notably, this phenomenon was not observed as a systematic bias of next-generation sequencing because the binding signals of SigE, SigA, and control showed no negative correlation to GC contents (Figure S4A). While 805 of 3614 genes overlapped with CyAbrB2 binding regions, almost half (399 of 805 genes) were entirely covered by CyAbrB2 binding regions. The CyAbrB2

binding regions included 80 of 125 insertion sequence elements (Figure 3D). Comparison with the transcriptome of *cyabrB2*Δ revealed CyAbrB2 tended to suppress the genes overlapping with its binding regions under aerobic conditions (Figures 3A and 3E). A survey of the genomic localization of CyAbrB1 under aerobic conditions revealed that CyAbrB1 and CyAbrB2 shared similar binding patterns (Figures 3A and S4B). Due to the essentiality of CyAbrB1, we did not perform transcriptome analysis on a CyAbrB1-disrupted strain.

Localization of CyAbrB2 became blurry under the microoxic condtion

When cells entered microoxic conditions, the relative binding signals in the CyAbrB2 binding regions typically declined (Figure S5A). However, the signal change did not necessarily indicate that CyAbrB2 binding declined under microoxic conditions because the relative signal was normalized by total immunoprecipitation reads. Rather, the CyAbrB2 binding pattern became uniform when the cells entered microoxic conditions. Notably, the total quantities of precipitated DNA by tagged CyAbrB2 did not decrease, and qPCR confirmed that the CyAbrB2 binding signal increased in all positions tested (Figure S5B and S5C). The protein amount of cyAbrB2 was not altered on entry to the mircooxic condtion (Figure S5D).

CyAbrB2 binds to transiently upregulated genes

The binding regions of CyAbrB2 overlapped 17 of 28 transiently upregulated genes, showing significant enrichment from all upregulated genes (Figure 3F). While CyAbrB2 covered the entire

length of insertion sequences and unknown proteins, its binding positions on other transient genes were diverse (Figure 3G). Specifically, the *hox* and *nifJ* operons had two distinct binding regions located at the transcription start sites (TSSs) and middle of operons, the *pntAB* operon had two binding regions in the middle and downstream of the operon, and the *nrtABCD* operon had one binding region downstream of the operon (Figure 3H). Upon entry into microoxic conditions, the CyAbrB2 binding signal became less specific, consistent with the general tendency.

Sigma factors SigE and SigA tend to bind CyAbrB2-free promoter regions regardless of GC contents

We searched for SigE and SigA binding sites under aerobic and microoxic conditions (Figures 4A and 4B, top and bottom). Although our peak-calling threshold ignored many minor binding summits, the SigE and SigA peaks identified in this study predominantly covered the previously identified peaks (Figure S2D), reproducing the previous study's conclusion (Kariyazono and Osanai 2022). In other words, SigE and the primary sigma factor SigA share localization on the promoters of housekeeping genes, but SigE exclusively binds to the promoters of its dependent genes. SigE and SigA binding signals tended to be weaker in the CyAbrB2 binding regions than in the CyAbrB2-free regions (Figure 4C). As CyAbrB2 prefers AT-rich regions, we examined whether the peak summits of SigE and SigA were located in regions with high GC contents. Unexpectedly, GC contents around the peak summits of SigE and SigA were lower than that of the whole genome (Figure 4D), and no

correlation was found between the GC content and binding signals of SigE and SigA (Figure S4A). When cells entered microoxic conditions, the binding signals of SigA and SigE were changed, although most of their peaks observed under aerobic conditions were present under microoxic conditions (Figure 4A).

Next, we focused on Sigma factor dynamics in transiently upregulated genes. SigE, but not SigA, binds at the TSS of *pntAB* under aerobic and microoxic conditions. Under aerobic conditions, SigE binding summits were not identified at the TSSs of the *hox* and *nifJ* operons. However, the SigE-specific binding summit appeared at the TSS of *nifJ* when cells entered microoxic conditions (Figure 4E middle). A bimodal peak of SigE was observed at the TSS of the *hox* operon, although the peak caller failed to recognize it as two peaks (Figure 4E bottom panel). One side of the bimodal peak near the TSS of the *hox* operon lacked SigA binding. These peaks are consistent with the notion that transiently upregulated genes, which are expressed in a SigE-dependent manner, belong to the *hox*, *nifJ*, and *pntAB* operons.

CyAbrB2-dependent and independent chromatin conformation around *hox* operon

We have shown that CyAbrB2 broadly binds to AT-rich genomic regions, including insertion element sequences, and represses expression (Figures 3B and 3D). This is functionally similar to the NAP family, which makes us hypothesize that cyAbrB2 modulates chromosomal conformation. Therefore, we conducted the chromatin conformation capture (3C) assay against wildtype and

cyAbrB2 deleted strains at aerobic and microoxic conditions (1hr and 4hr). qPCR was performed with unidirectional primer sets, and the genomic fragment containing *hox* operon (hereinafter hox fragment) as bait (Figure 5A). We then observed that the hox fragment interacted with its distal downstream region and proximal upstream region in the aerobic condition (Figure 5B and 5C, locus(c) and (j)). Those interactions were detected both in wildtype and *cyabrb2*Δ. Moreover, the interaction frequency between the hox fragment and its distal downstream was higher in wildtype than *cyabrb2*Δ.

CyabrB2 mediates chromatin conformation changes upon microoxic condition.

When the wildtype cells entered the microoxic condition, the *hox* fragment diminished its interaction with its distal downstream and proximal upstream region (Figure 5B locus(c) and (j)). Such decrement of interaction was not observed in *cyabrb2*Δ mutant. While the interaction scores exhibit considerable variability, the individual data over time demonstrate declining trends of the wildtype at locus (c) and (j) (Figure S7). Furthermore, both of wildtype and *ayabrb2*Δ mutant showed increased interaction with the proximal downstream fragments on entry to the microoxic conditions (Figure 5B and 5C, locus (f),(g),(h)).In the wildtype cells, the interaction with locus (g) was transiently elevated at 1hour of the microoxic condition, but decreased to the aerobic level. In summary, 3C analysis revealed cyAbrB2-dependent and independent dynamics of chromosomal conformation around *hox* operon in response to the

microoxic condition (Figure 5D).

Discussion

Physiological significance of transient upregulation of *hox* and *nifJ* operons

Time-course transcriptome analysis revealed that the *hox* and *nifJ* operons were transiently upregulated under microoxic conditions. The reasons for transient upregulation may be due to the limited number of inorganic cofactors and the reusability of fermentative products. Hydrogenase and NifJ proteins have iron–sulfur clusters, and cyanobacterial hydrogenase requires nickel for its activity (Uyeda and Rabinowitz 1971; Vignais and Billoud 2007). Continuous expression of the *hox* gene is futile under physiological conditions, as the overexpression of this gene does not yield a proportional increase in hydrogenase activity without an adequate nickel supply (Ortega-Ramos et al. 2014). Furthermore, hydrogenase-produced hydrogen is diffusive and thus difficult to reuse as reducing power when cells return to aerobic conditions. Unlike hydrogen fermentation, the reverse tricarboxylic acid (rTCA) cycle produces dicalboxic acids, which are reusable for generating NADPH via the TCA cycle under aerobic conditions (Katayama et al. 2022). However, adding bicarbonate to phosphoenolpyruvate (PEP) is a rate-limiting step in the rTCA cycle (Hasunuma, Matsuda, and Kondo 2016). Hydrogenase may favor fermentation initiation since it uses only protons as a substrate, and the rTCA cycle may become active subsequently. We classified the gene expression of *citH*/*mdh* (sll0891) encoding a key enzyme of the rTCA cycle as continuously

upregulated genes (Figure 1D).

Significance of multiple regulations of hydrogenase expression

H_2 fermentation is beneficial when the reducing power is in excess, the rTCA cycle is less active, and electron acceptors such as oxygen and nitrate are absent. When SigE and CyAbrB2 work, cells are in the midst of such conditions. In particular, SigE is transcriptionally upregulated under nitrogen starvation, which means low nitrate conditions, and posttranscriptionally activated in the dark, meaning the Calvin cycle is inactive (Muro-Pastor, Herrero, and Flores 2001; Osanai et al. 2009). Because SigE transcribes genes involved in catalyzing the glycogen catabolism, glycolysis, and oxidative pentose phosphate pathway (Osanai et al. 2011), activation of SigE prmotes production of reducing power. CyAbrB2 and LexA respond to low CO_2 conditions (Domain et al. 2004; Lieman-Hurwitz et al. 2009; Orf et al. 2016) under which PEP carboxylation is slower, resulting in rTCA limitation. Our results demonstrate that CyAbrB2 responds to low oxygen. and that multiple environmental signals are integrated into the *hox* promoter through the dynamics of CyAbrB2, LexA, and SigE.

Three types of the localization pattern and function of cyAbrB2

We classified three types of binding patterns for cyAbrB2 based on the ChIP-seq data of cyAbrB2. The first pattern is that cyAbrB2 binds a long tract of DNA covering the entire gene or operon, represented by the insertion sequence elements. cyAbrB2 tends to suppress the

expression at this pattern (Figure 3D and 3E). The second pattern is binding on promoter regions, such as *hox* operon and *nifJ*. cyAbrB2 binding on those promoters fluctuates in response to environmental changes, thus regulating expression. This pattern also applies to the promoter of *sbtA* (Na^+/HCO_3^- symporter), as the previous study reported that cyAbrB2 is bound to the *sbtA* promoter in a CO_2 concentration-dependent manner (Lieman-Hurwitz et al. 2009). The last one is that cyAbrB2 binds at the middle or downstream of operons. The middle of *hox*, *pntAB*, and *nifJ* operons and the downstream of *nrt* operon are the cases (Figure 3G). We observed that genes in the same operon separated by the cyAbrB2 binding region behave differently. In particular, *pntB* is classified as the transiently upregulated gene, while *pntA* is not, despite being in the same operon. This mgiht be explained by the recent study reported cyAbrB2 affets the stability of mRNA transcribed from its binding gene (Song et al. 2022). Hereafter, we will focus on the mechanism of the second pattern, regulation by cyAbrB2 on the promoter.

Insights into transcriptional regulation of *hox* operon and *nifJ*

Genome wide analysis revealed that SigE and SigA binding signals are low in the cyAbrB2 binding region (Figure 4C), suggesting that the CyAbrB2-bound region seems to block SigE and SigA. This is presumably because sigma factors recognize the promoter as a large complex of RNA polymerase and thus require promoter accessibility. CyAbrB2 binds to the *hox and nifJ* promoter region and may inhibit access to the RNA polymerase complex under aerobic conditions. When cells

entered microoxic conditions, the binding pattern of cyAbrB2 on the *hox* and *nifJ* promoters got less specific, and SigE binding peaks on those promoters became prominent (Figure 4E). It is of note that cyAbrB2 ChIP efficiency at the *hox* promoter is higher in the microoxic condtion than the aerobic condtion (Figure S5C). Therefore, the mechanism by which cyAbrB2 inhibits SigE-containing RNAP in the aerobic condtion is not solely based on exclusion by occupancy. Rather,

A possible mechanism for cyAbrB2-mediated chromosomal conformation

3C analysis suggested that cyAbrB2 mediates the interaction between the hox fragment and distal downstream region (Figure 5A and 5B, locus (c)). The hox promoter region possesses cyAbrB2 binding region, and locus (c) is adjacent to cyAbrB2 binding region. Therefore, cyAbrB2 may mediate chromosomal conformation by bridging its binding regions, like the typical NAPs such as H-NS do. However, no biochemical data mentioned DNA bridging function of cyAbrB2 in the previous studies (Dutheil et al. 2012; Ishii and Hihara 2008; Song et al. 2022). CyAbrB1, the homolog of cyAbrB2, may cooperatively work, as cyAbrB1 directly interacts with cyAbrB2 (Yamauchi et al. 2011), and their distribution is similar. In the microoxic condition, cyAbrB2 binding became blurry, which might reduce the specific interaction between the hox region and locus (c). On the other hand, cyAbrB2 indirectly mediates interaction with its proximal upstream region (Figure 5B, locus (j)), as this region is devoid of cyAbrB2 binding (Figure 5A locus (i) to (l)).

Correlation between chromosomal conformation and transcriptional regulation

The conformational change correlates with the expression level of *hox* operon, though further investigations are needed to establish causality. Specifically, the interaction between the hox operon and its proximal downstream region showed transient elevation upon entry to the microoxic condition (Figure 5B, locus (f) and (g)), corresponding to the transient expression of hox operon. Similarly, loss of interaction between the hox fragment and its upstream region (locus (j)) under the microoxic condition may reflect expression change in the hox operon. Moreover, Song et al. pointed out that DNA looping may inhibit transcription (Song et al. 2022) because artificial DNA looping by the LacI repressor of *E. coli* can repress cyanobacterial transcription (Camsund, Heidorn, and Lindblad 2014).

Chromosomal conformation change in cyanobacteria

Our 3C analysis revealed that local chromosomal conformation change upon entry to the microoxic conditions. The conformational changes occur in both AbrB2-dependent and AbrB2-independent manners. Cyanobacteria face various environmental changes besides the microoxic condition, and there are potential NAPs in cyanobacteria yet to be characterized. Therefore, we speculate that conformational change of the entire chromosome occurs to deal with anaerobiosis, high light, osmotic stress, and nutrient depletion.

Unrevealed mechanism for the downregulation of *hox* operon and *nifJ*

We have proposed the mechanism for activating *hox* operon and *nifJ* on entry to the microoxic condition mediated by SigE and cyAbrB2. However, cyAbrB2 and SigE are insufficient to explain the decline of *hox* and *nifJ* expression at 4-hour cultivation of the microoxic condition. RT-qPCR reported that the expression of *hoxF* and *nifJ* dropped at 4-hour microoxic condition cultivation, even in the absence of cyAbrB2 or SigE.

Roles of CyAbrB2 beyond the regulation of fermentative genes

CyAbrB2 deletion has been shown to decrease several genes regulated by NtcA, the global transcriptional regulator of nitrogen metabolism (Ishii and Hihara 2008), and genes regulated by NdhR and CmpR, the transcriptional regulator of the carbon-concentrating mechanism (Orf et al. 2016). CyAbrB2 may support these transcription factors by modulating chromatin conformation.

The CyAbrB family is widely conserved in cyanobacteria. A recent study on heterocyst-forming cyanobacteria implicated the CyAbrB2 homolog in heterocyst differentiation (Higo et al. 2019). CalA, a CyAbrB2 homolog in *Anabaena* sp. PCC7120, represses *hetP* and *hepA*, genes required for heterocyst formation. *HetP* and *hepA* are also upregulated by hetR, the master regulator of heterocyst differentiation. HetR regulates *hetP* and *hepA*, independent of CalA/CyAbrB2, which is analogous to the *hox* gene regulation in *Synechocystis*. Therefore, CyAbrB2-mediated chromatin conformation may govern various cyanobacterial regulations, ranging from the fermentative gene's transcription to heterocyst differentiation.

EXPERIMENTAL PROCEDURES

Bacterial strains and plasmids

The glucose-tolerant strain of *Synechocystis* sp. PCC6803 (Williams 1988) was used as a wildtype strain in this study. The SigE (sll1689)-disrupted strain (G50) was constructed in a previous study (Osanai et al. 2005). Disruption and epitope-tagging of abrB1(*sll0359*) and abrB2(*sll0822*) were performed by homologous double recombination between the genome and PCR fragment (Williams 1988). The resulting transformants were selected using three passages on BG-11 plates containing 5 µg/mL kanamycin. Genomic PCR was used to confirm the insertion of epitope tag fragments and gene disruption (Figure S2A). Supplemental Tables S1, S2, and S3 contain the cyanobacterial strains, oligonucleotides, and plasmids used in this study.

Aerobic and microoxic culture conditions

For aerobic conditions, cells were harvested after 24-h cultivation in HEPES-buffered BG-11_0 medium (Rippka, Deruelles, and Waterbury 1979), which was buffered with 20 mM HEPES-KOH (pH 7.8) containing 5 mM NH_4Cl under continuous exposure to white light (40 µmol $m^{-2}s^{-1}$) and bubbled with air containing 1% CO_2 (final OD_{730} = 1.4–1.8). For the dark anaerobic culture, the aerobic culture cell was concentrated to an OD_{730} of 20 with the centrifuge and resuspended in the culture medium. The concentrated cultures were poured into vials, bubbled

with N_2 gas, and sealed. The sealed vials were shaded and shaken at 30˚C for the described times.

Antibodies and immunoblotting

Sample preparation for immunoblotting was performed as previously described (Kariyazono and Osanai 2022), and FLAG-tagged proteins were detected by alkaline-phosphatase-conjugated anti-FLAG IgG (A9469, Sigma Aldrich) and 1-Step™ NBT/BCIP substrate solution (Thermo Fisher Scientific, Waltham, MA).

RNA isolation

Total RNA was isolated with ISOGEN (Nippon gene) following the manufacturer's instructions and stored at −80˚C until use. We prepared triplicates for each timepoint for the RNA-seq library.

ChIP assay

Two biological replicates were used for each ChIP-seq experiment, and one untagged control ChIP was performed. ChIP and qPCR analyses were performed using the modified version of a previous method (Kariyazono and Osanai 2022). FLAG-tagged proteins were immunoprecipitated with FLAG-M2 antibody (F1804 Sigma-Aldrich) conjugated to protein G dynabeads (10003D Invitrogen).

Genome extraction, digestion, and ligation for 3C assay

3C assay was conducted based on the previous prokaryotic Hi-C experiment (Takemata and Bell 2021; Takemata, Samson, and Bell 2019), with certain steps modified. Briefly, *Synechocystis* were fixed by 2.5% formaldehyde for 15 minutes at room temperature. Fixation was terminated by adding a final concentration of 0.5M of glycine, and cells were stored at -80˚C until use. Fixed cells were disrupted using glass beads and shake master® NEO (Bio Medical Science, Tokyo, Japan), as described in the previous study's section on preparing cell lysate for ChIP. The lysates were incubated with buffer containing 1mM Tris-HCl (pH7.5), 0.1mM EDTA, and 0.5% SDS for 10min at room temperature, and 1% Triton X-100 quenched SDS. Genomes in the cell lysate were digested by 600U/mL of HindIII (Takara) for 4 hours at 37˚C, and RNA in the lysate was simultaneously removed by 50μg/mL of RNAseA (Nippon genetics). The digestion was terminated by adding 1% SDS and 22 mM EDTA. The fill-in reaction and biotin labeling steps were omitted from the procedure. The digested genomes were diluted by ligation buffer containing 1% triton-X100 to the final concentration of approximately 1μg/mL and incubated for 10 min at room temperature. Ligation was performed with 2U/mL of T4 DNA ligase (Nippon Gene) overnight at 16˚C. Crosslinking was reversed under 65˚C for 4 hours in the presence of 2.5mg/mL of proteinase K (Kanto Chemical), and DNA was purified with the phenol-chloroform method and ethanol precipitation method.

Preparation of calibration samples for 3C qPCR

Based on a previous study, calibration samples for possible ligated pairs were prepared in parallel with 3C ligation (Abou El Hassan and Bremner 2009). In brief, the purified genome of *Synechocystis* was digested by HindIII, and DNA was purified with the phenol-chloroform and ethanol precipitation. Purified DNA was dissolved into the water at a concentration of about 600ng/µL and ligated with 2U/mL of T4 DNA ligase at 16˚C overnight. As a result, DNA ~600-fold condensed DNA than 3C samples were ligated.

Quantification of crosslinking frequency for 3C assay

Before Real-time PCR assay, we confirmed that each primer set amplified single bands in a ligation dependent manner by GoTaq® Hot Start Green Master Mix (Promega,Madison,WI) (Figure S6). Real-time PCR was performed with StepOnePlus™ (Applied Biosystems, Foster City, CA) and Fast SYBR™ Green Master Mix (Thermo Fisher Scientific) according to the manufacturer's instructions. Interaction frequency was quantified by ΔΔCt method using dilution series of calibration samples described above. We confirmed each primer set amplified DNA fragment with a unique Tm value. We also quantified the amount of the bait fragment containing *hox* operon as an internal control. Supplemental table S2 contains the list of primers used in the 3C quantification. Interaction frequency for each primer position was calculated as the relative abundance of ligated fragments against the calibration samples and normalized among samples by internal control.

Library preparation and next-generation sequencing

For the ChIP-seq library, input and immunoprecipitated DNA were prepared into multiplexed libraries using either NEBNEXT (E7645 New England Biolabs). For the RNA-seq library, isolated RNA samples were deprived of ribosomal RNA with Illumina Ribo-Zero Plus rRNA Depletion Kit (20040526 Illumina) and processed into a cDNA library for Illumina with the NEBNext Ultra II Directional RNA Library Prep Kit for Illumina (E7760 New England Biolabs). Dual-index primers were conjugated with NEBNext Multiplex Oligos for Illumina (E6440S New England Biolabs). We pooled all libraries, and the multiplexed libraries were dispatched to Macrogen Japan Inc. and subjected to paired-end sequencing with HiSeqX. Adapter trimming and quality filtering of raw sequence reads were conducted with fastp (ver. 0.21.0) (Chen et al. 2018) under default conditions. The paired-end sequences were mapped onto the *Synechocystis* genome (ASM972v1) using Bowtie2 (Langmead and Salzberg 2012) (ver. 2.4.5 paired-end). Supplementary Table S4 contains the read counts that passed via fastp quality control and were mapped by Bowtie2.

RNA-seq analysis

Mapped reads were counted by HT-seq count (ver. 2.0.2)(Anders, Pyl, and Huber 2015) for the GFF file of ASM972v1, with the reverse-strandedness option. EdgeR package (ver. 3.40.1)(Robinson, McCarthy, and Smyth 2010) was used to perform the differential expression

analysis. Fold changes in expression and FDR were used for gene classification. Supplemental Table S5-S7 contains fold change in gene expression calculated by edgeR.

Genome-wide analyses

Peaks were called using the MACS3 program (ver. 3.0.0b1) (Zhang et al. 2008). For paired-end reads for SigE, SigA, and untagged control ChIP, narrow peaks were called with <1e−20 of the q-value cut-off and "--call-summits" options. The peak summits from two replicates and the untagged control were merged if summits were located within 40 bp of each other. Peak summits identified in both replicates, but not in the control, were considered for further analysis. The midpoint of the peak summits for the two merged replicates was further analyzed.

Broad peak calling methods were applied to paired-end reads for CyAbrB2, CyAbrB1, and untagged control ChIP using the "–broad" option, with a q-value cut-off of < 0.05 and a q-value broad cut-off of < 0.05. The intersection of broad peaks from two replicates excluding those called by the control was used in subsequent analyses.

The positions of the TSS, including internal start sites, were obtained as reported by Kopf et al. (2014). The read count, merging, and the intersection of the binding region were calculated using BEDTools (ver. 2.30.0) (Quinlan and Hall 2010). Supplemental Tables S8–S14 contain SigA and SigE peaks and the broad binding regions of CyAbrB2 and CyAbrB1, respectively.

Binding signals in every 100 bp bin for scatter plots were calculated as (IP read counts within

100 bp window) / (input read counts within 100 bp window) * (total input read counts/total IP read counts). GC contents were calculated within 500 bp in 100 bp sliding windows by seqkit (ver. 2.3.0) [42].

Statistical analysis

Statistical analyses were performed with R version 4.2.2 (Anon 2022). The “fisher.test” function was used for Fisher’s exact test, and p-values < 0.05 were denoted as asterisks in the figure. Multiple comparisons of Fisher's exact test were conducted using “Fisher. multcomp” function in the RVAideMemoire package (Hervé 2022), where P-values were adjusted by the “fdr” method and FDRs <0.05 are shown in the figures. Multiple comparisons of the Wilcoxon-rank test were conducted by “pairwise.wilcox.test,” and p-values were adjusted by the “fdr” method. Adjusted p-values < 0.05 are shown in the figure. The correlation coefficient was calculated with the “cor” function. Gene set enrichment analysis (GSEA) was perfromed by culsterPlofiler package (Wu et al. 2021) in R with p-value cut-off of 0.05. The enriched pathways detected by GSEA are listed in Supplemental Tables S15.

ACCESSION NUMBERS

Raw ChIP sequencing and RNA sequencing reads were deposited in the Sequence Read Archive (accession ID: PRJNA956842).

Conflicts of interest

There were no conflicts of interest to declare.

Acknowledgments

This study was supported by the following grants to T.O.: Grant-in-Aid for Scientific Research (B) (grant no. 20H02905) and JST-ALCA of the Japan Science and Technology Agency (grant number JPMJAL1306). We thank Dr. Kohki Yoshimoto for providing laboratory instruments and Ms. Kaori Iwazumi for the support of bacterial culture and the medium preparation.

Author contributions

RK and TO designed the study; RK conducted the experiment; RK analyzed the data; RK and TO wrote the paper.

References

Abou El Hassan, M. and R. Bremner. 2009. "A Rapid Simple Approach to Quantify Chromosome Conformation Capture." *Nucleic Acids Research* 37(5):e35.

Anders, Simon, Paul Theodor Pyl, and Wolfgang Huber. 2015. "HTSeq--a Python Framework to Work with High-Throughput Sequencing Data." *Bioinformatics (Oxford, England)* 31(2):166–69.

Anon. 2022. "R: A Language and Environment for Statistical Computing."

Appel, J., S. Phunpruch, K. Steinmüller, and R. Schulz. 2000. "The Bidirectional Hydrogenase of

Synechocystis Sp. PCC 6803 Works as an Electron Valve during Photosynthesis." *Archives of Microbiology* 173(5–6):333–38.

Artz, Jacob H., Monika Tokmina-Lukaszewska, David W. Mulder, Carolyn E. Lubner, Kirstin Gutekunst, Jens Appel, Brian Bothner, Marko Boehm, and Paul W. King. 2020. "The Structure and Reactivity of the HoxEFU Complex from the Cyanobacterium Synechocystis Sp. PCC 6803." *The Journal of Biological Chemistry* 295(28):9445–54.

Camsund, Daniel, Thorsten Heidorn, and Peter Lindblad. 2014. "Design and Analysis of LacI-Repressed Promoters and DNA-Looping in a Cyanobacterium." *Journal of Biological Engineering* 8(1):4.

Carrieri, Damian, Karen Wawrousek, Carrie Eckert, Jianping Yu, and Pin-Ching Maness. 2011. "The Role of the Bidirectional Hydrogenase in Cyanobacteria." *Bioresource Technology* 102(18):8368–77.

Cassier-Chauvat, Corinne, Théo Veaudor, and Franck Chauvat. 2014. "Advances in the Function and Regulation of Hydrogenase in the Cyanobacterium Synechocystis PCC6803." *International Journal of Molecular Sciences* 15(11):19938–51.

Chen, Shifu, Yanqing Zhou, Yaru Chen, and Jia Gu. 2018. "Fastp: An Ultra-Fast All-in-One FASTQ Preprocessor." *Bioinformatics* 34(17):i884–90.

Domain, Francis, Laetitia Houot, Franck Chauvat, and Corinne Cassier-Chauvat. 2004. "Function and Regulation of the Cyanobacterial Genes LexA, RecA and RuvB: LexA Is Critical to the Survival of

Cells Facing Inorganic Carbon Starvation." *Molecular Microbiology* 53(1):65–80.

Dutheil, Jérémy, Panatda Saenkham, Samer Sakr, Christophe Leplat, Marcia Ortega-Ramos, Hervé Bottin, Laurent Cournac, Corinne Cassier-Chauvat, and Franck Chauvat. 2012. "The AbrB2 Autorepressor, Expressed from an Atypical Promoter, Represses the Hydrogenase Operon to Regulate Hydrogen Production in Synechocystis Strain PCC6803." *Journal of Bacteriology* 194(19):5423–33.

Gutekunst, Kirstin, Xi Chen, Karoline Schreiber, Ursula Kaspar, Srinivas Makam, and Jens Appel. 2014. "The Bidirectional NiFe-Hydrogenase in Synechocystis Sp. PCC 6803 Is Reduced by Flavodoxin and Ferredoxin and Is Essential under Mixotrophic, Nitrate-Limiting Conditions." *The Journal of Biological Chemistry* 289(4):1930–37.

Gutekunst, Kirstin, Saranya Phunpruch, Christoph Schwarz, Sven Schuchardt, Rüdiger Schulz-Friedrich, and Jens Appel. 2005. "LexA Regulates the Bidirectional Hydrogenase in the Cyanobacterium Synechocystis Sp. PCC 6803 as a Transcription Activator." *Molecular Microbiology* 58(3):810–23.

Hasunuma, Tomohisa, Mami Matsuda, and Akihiko Kondo. 2016. "Improved Sugar-Free Succinate Production by Synechocystis Sp. PCC 6803 Following Identification of the Limiting Steps in Glycogen Catabolism." *Metabolic Engineering Communications* 3:130–41.

Hervé, Maxime. 2022. "RVAideMemoire: Testing and Plotting Procedures for Biostatistics."

Higo, Akiyoshi, Eri Nishiyama, Kota Nakamura, Yukako Hihara, and Shigeki Ehira. 2019. "CyAbrB Transcriptional Regulators as Safety Devices To Inhibit Heterocyst Differentiation in Anabaena Sp.

Strain PCC 7120." *Journal of Bacteriology* 201(17).

Hołówka, Joanna and Jolanta Zakrzewska-Czerwińska. 2020. "Nucleoid Associated Proteins: The Small Organizers That Help to Cope With Stress." *Frontiers in Microbiology* 11:590.

Iijima, Hiroko, Tomokazu Shirai, Mami Okamoto, Filipe Pinto, Paula Tamagnini, Tomohisa Hasunuma, Akihiko Kondo, Masami Yokota Hirai, and Takashi Osanai. 2016. "Metabolomics-Based Analysis Revealing the Alteration of Primary Carbon Metabolism by the Genetic Manipulation of a Hydrogenase HoxH in Synechocystis Sp. PCC 6803." *Algal Research* 18:305–13.

Iijima, Hiroko, Atsuko Watanabe, Haruna Sukigara, Kaori Iwazumi, Tomokazu Shirai, Akihiko Kondo, and Takashi Osanai. 2021. "Four-Carbon Dicarboxylic Acid Production through the Reductive Branch of the Open Cyanobacterial Tricarboxylic Acid Cycle in Synechocystis Sp. PCC 6803." *Metabolic Engineering* 65:88–98.

Imamura, Sousuke and Munehiko Asayama. 2009. "Sigma Factors for Cyanobacterial Transcription." *Gene Regulation and Systems Biology* 3:65–87.

Ishii, Ai and Yukako Hihara. 2008. "An AbrB-like Transcriptional Regulator, Sll0822, Is Essential for the Activation of Nitrogen-Regulated Genes in Synechocystis Sp. PCC 6803." *Plant Physiology* 148(1):660–70.

Kariyazono, Ryo and Takashi Osanai. 2022. "Identification of the Genome-Wide Distribution of Cyanobacterial Group-2 Sigma Factor SigE, Accountable for Its Regulon." *The Plant Journal*□*:*

For Cell and Molecular Biology 110(2):548–61.

Katayama, Noriaki, Kaori Iwazumi, Hiromi Suzuki, Takashi Osanai, and Shoki Ito. 2022. "Malic Enzyme, Not Malate Dehydrogenase, Mainly Oxidizes Malate That Originates from the Tricarboxylic Acid Cycle in Cyanobacteria." *MBio* 13(6):e0218722.

Kopf, Matthias, Stephan Klähn, Nadin Pade, Christian Weingärtner, Martin Hagemann, Björn Voß, and Wolfgang R. Hess. 2014. "Comparative Genome Analysis of the Closely Related Synechocystis Strains PCC 6714 and PCC 6803." *DNA Research : An International Journal for Rapid Publication of Reports on Genes and Genomes* 21(3):255–66.

Langmead, Ben and Steven L. Salzberg. 2012. "Fast Gapped-Read Alignment with Bowtie 2." *Nature Methods* 9(4):357–59.

Leplat, Christophe, Raphaël Champeimont, Panatda Saenkham, Corinne Cassier-Chauvat, Aude Jean-Christophe, and Franck Chauvat. 2013. "Genome-Wide Transcriptome Analysis of Hydrogen Production in the Cyanobacterium Synechocystis: Towards the Identification of New Players." *International Journal of Hydrogen Energy* 38(4):1866–72.

Lieman-Hurwitz, Judy, Maya Haimovich, Gali Shalev-Malul, Ai Ishii, Yukako Hihara, Ariel Gaathon, Mario Lebendiker, and Aaron Kaplan. 2009. "A Cyanobacterial AbrB-like Protein Affects the Apparent Photosynthetic Affinity for CO2 by Modulating Low-CO2-Induced Gene Expression." *Environmental Microbiology* 11(4):927–36.

McNeely, Kelsey, Yu Xu, Nick Bennette, Donald A. Bryant, and G. Charles Dismukes. 2010. "Redirecting Reductant Flux into Hydrogen Production via Metabolic Engineering of Fermentative Carbon Metabolism in a Cyanobacterium." *Applied and Environmental Microbiology* 76(15):5032–38.

Muro-Pastor, A. M., A. Herrero, and E. Flores. 2001. "Nitrogen-Regulated Group 2 Sigma Factor from Synechocystis Sp. Strain PCC 6803 Involved in Survival under Nitrogen Stress." *Journal of Bacteriology* 183(3):1090–95.

Oliveira, Paulo and Peter Lindblad. 2005. "LexA, a Transcription Regulator Binding in the Promoter Region of the Bidirectional Hydrogenase in the Cyanobacterium Synechocystis Sp. PCC 6803." *FEMS Microbiology Letters* 251(1):59–66.

Oliveira, Paulo and Peter Lindblad. 2008. "An AbrB-Like Protein Regulates the Expression of the Bidirectional Hydrogenase in Synechocystis Sp. Strain PCC 6803." *Journal of Bacteriology* 190(3):1011–19.

Orf, Isabel, Doreen Schwarz, Aaron Kaplan, Joachim Kopka, Wolfgang R. Hess, Martin Hagemann, and Stephan Klähn. 2016. "CyAbrB2 Contributes to the Transcriptional Regulation of Low CO2 Acclimation in Synechocystis Sp. PCC 6803." *Plant and Cell Physiology* 57(10):2232–43.

Ortega-Ramos, Marcia, Thichakorn Jittawuttipoka, Panatda Saenkham, Aurelia Czarnecka-Kwasiborski, Hervé Bottin, Corinne Cassier-Chauvat, and Franck Chauvat. 2014. "Engineering Synechocystis

PCC6803 for Hydrogen Production: Influence on the Tolerance to Oxidative and Sugar Stresses." *PloS One* 9(2):e89372.

Osanai, Takashi, Masahiko Imashimizu, Asako Seki, Shusei Sato, Satoshi Tabata, Sousuke Imamura, Munehiko Asayama, Masahiko Ikeuchi, and Kan Tanaka. 2009. "ChlH, the H Subunit of the Mg-Chelatase, Is an Anti-Sigma Factor for SigE in Synechocystis Sp. PCC 6803." *Proceedings of the National Academy of Sciences of the United States of America* 106(16):6860–65.

Osanai, Takashi, Yu Kanesaki, Takayuki Nakano, Hiroyuki Takahashi, Munehiko Asayama, Makoto Shirai, Minoru Kanehisa, Iwane Suzuki, Norio Murata, and Kan Tanaka. 2005. "Positive Regulation of Sugar Catabolic Pathways in the Cyanobacterium Synechocystis Sp. PCC 6803 by the Group 2 Sigma Factor SigE." *The Journal of Biological Chemistry* 280(35):30653–59.

Osanai, Takashi, Akira Oikawa, Miyuki Azuma, Kan Tanaka, Kazuki Saito, Masami Yokota Hirai, and Masahiko Ikeuchi. 2011. "Genetic Engineering of Group 2 Sigma Factor SigE Widely Activates Expressions of Sugar Catabolic Genes in Synechocystis Species PCC 6803." *The Journal of Biological Chemistry* 286(35):30962–71.

Osanai, Takashi, Tomokazu Shirai, Hiroko Iijima, Yuka Nakaya, Mami Okamoto, Akihiko Kondo, and Masami Y. Hirai. 2015. "Genetic Manipulation of a Metabolic Enzyme and a Transcriptional Regulator Increasing Succinate Excretion from Unicellular Cyanobacterium ." *Frontiers in Microbiology* 6:1064.

Puggioni, Vincenzo, Sébastien Tempel, and Amel Latifi. 2016. “Distribution of Hydrogenases in Cyanobacteria: A Phylum-Wide Genomic Survey.” *Frontiers in Genetics* 7:223.

Quinlan, Aaron R. and Ira M. Hall. 2010. “BEDTools: A Flexible Suite of Utilities for Comparing Genomic Features.” *Bioinformatics* 26(6):841–42.

Rippka, R., J. Deruelles, and J. B. Waterbury. 1979. “Generic Assignments, Strain Histories and Properties of Pure Cultures of Cyanobacteria.” *Journal of General Microbiology* 111(1):1–61.

Robinson, Mark D., Davis J. McCarthy, and Gordon K. Smyth. 2010. “EdgeR: A Bioconductor Package for Differential Expression Analysis of Digital Gene Expression Data.” *Bioinformatics (Oxford, England)* 26(1):139–40.

Shen, Wei, Shuai Le, Yan Li, and Fuquan Hu. 2016. “SeqKit: A Cross-Platform and Ultrafast Toolkit for FASTA/Q File Manipulation.” *PloS One* 11(10):e0163962.

Song, Kuo, Martin Hagemann, Jens Georg, Sandra Maaß, Dörte Becher, and Wolfgang R. Hess. 2022. “Expression of the Cyanobacterial F(o)F(1) ATP Synthase Regulator AtpΘ Depends on Small DNA-Binding Proteins and Differential MRNA Stability.” *Microbiology Spectrum* 10(3):e0256221.

Stal, Lucas J. and Roy Moezelaar. 1997. “Fermentation in Cyanobacteria1Publication 2274 of the Centre of Estuarine and Coastal Ecology, Yerseke, The Netherlands.1.” *FEMS Microbiology Reviews* 21(2):179–211.

Summerfield, Tina C., Sowmya Nagarajan, and Louis A. Sherman. 2011. “Gene Expression under Low-

Oxygen Conditions in the Cyanobacterium Synechocystis Sp. PCC 6803 Demonstrates Hik31-Dependent and -Independent Responses." *Microbiology (Reading, England)* 157(Pt 2):301–12.

Takemata, Naomichi and Stephen D. Bell. 2021. "Chromosome Conformation Capture Assay Combined with Biotin Enrichment for Hyperthermophilic Archaea." *STAR Protocols* 2(2):100576.

Takemata, Naomichi, Rachel Y. Samson, and Stephen D. Bell. 2019. "Physical and Functional Compartmentalization of Archaeal Chromosomes." *Cell* 179(1):165-179.e18.

Uyeda, K. and J. C. Rabinowitz. 1971. "Pyruvate-Ferredoxin Oxidoreductase. 3. Purification and Properties of the Enzyme." *The Journal of Biological Chemistry* 246(10):3111–19.

Vignais, Paulette M. and Bernard Billoud. 2007. "Occurrence, Classification, and Biological Function of Hydrogenases: An Overview." *Chemical Reviews* 107(10):4206–72.

Williams, John G. K. 1988. "Construction of Specific Mutations in Photosystem II Photosynthetic Reaction Center by Genetic Engineering Methods in Synechocystis 6803." Pp. 766–78 in *Methods in Enzymology*. Vol. 167. Academic Press.

Wu, Tianzhi, Erqiang Hu, Shuangbin Xu, Meijun Chen, Pingfan Guo, Zehan Dai, Tingze Feng, Lang Zhou, Wenli Tang, Li Zhan, Xiaocong Fu, Shanshan Liu, Xiaochen Bo, and Guangchuang Yu. 2021. "ClusterProfiler 4.0: A Universal Enrichment Tool for Interpreting Omics Data." *Innovation (Cambridge (Mass.))* 2(3):100141.

Yamauchi, Yuki, Yuki Kaniya, Yasuko Kaneko, and Yukako Hihara. 2011. "Physiological Roles of the

CyAbrB Transcriptional Regulator Pair Sll0822 and Sll0359 in Synechocystis Sp. Strain PCC 6803." *Journal of Bacteriology* 193(15):3702–9.

Zhang, Yong, Tao Liu, Clifford A. Meyer, Jérôme Eeckhoute, David S. Johnson, Bradley E. Bernstein, Chad Nusbaum, Richard M. Myers, Myles Brown, Wei Li, and X. Shirley Liu. 2008. "Model-Based Analysis of ChIP-Seq (MACS)." *Genome Biology* 9(9):R137.

Table 1 List of transiently upregulated genes

		Operon
Oxidoreductase		
sll0741	nifJ/"pyruvate-ferredoxin/flavodoxin oxidoreductase"	TU3296
sll0743	hypothetical protein	
sll0744	dihydroorotate dehydrogenase (fumarate)	
sll1221	hoxF/"bidirectional [NiFe] hydrogenase diaphorase subunit"	TU1714
sll1222	unknown protein	
sll1223	hoxU/"bidirectional [NiFe] hydrogenase diaphorase subunit"	
sll1224	hoxY/"NAD-reducing hydrogenase small subunit"	
sll1225	unknown protein	
sll1226	hoxH/"NAD-reducing hydrogenase large subunit"	
slr1434	pntB/"H+-translocating NAD(P) transhydrogenase subunit beta"	TU1089
Transporter		
sll1450	nrtA/"nitrate/nitrite transport system substrate-binding protein"	TU1023
sll1451	nrtB/"nitrate/nitrite transport system permease protein"	
sll1452	nrtC/"nitrate/nitrite transport system ATP-binding protein"	
sll1453	nrtD/"nitrate/nitrite transport system ATP-binding protein"	
Two-component system		
slr1214	twitching motility two-component system response regulator PilG	TU905
slr1215	unknown protein	TU907
Glycosyl transferase		
slr2116	spsA/"spore coat polysaccharide biosynthesis protein; SpsA"	TU1673

Protease		
sll1009	frpC/"iron-regulated protein"	TU491
Insertion sequence (Transposase)		
slr1523	transposase	TU1659
sll1985	transposase	TU1589
sll7001	transposase	NA
sll7003	toxin FitB	TU7001
ssl0172	transposase	TU3163
Other		
slr1260	hypothetical protein	TU1446
slr0668	unknown protein	TU3532
slr5127	unknown protein	TU5127
sll0710	unknown protein	TU97
sll1307	unknown protein	TU1224

The list of transiently upregulated genes was merged by transcriptional units and sorted by function. The transcriptional unit information was obtained from a previous study (Kopf et al., 2014).

Figures and Figure legends

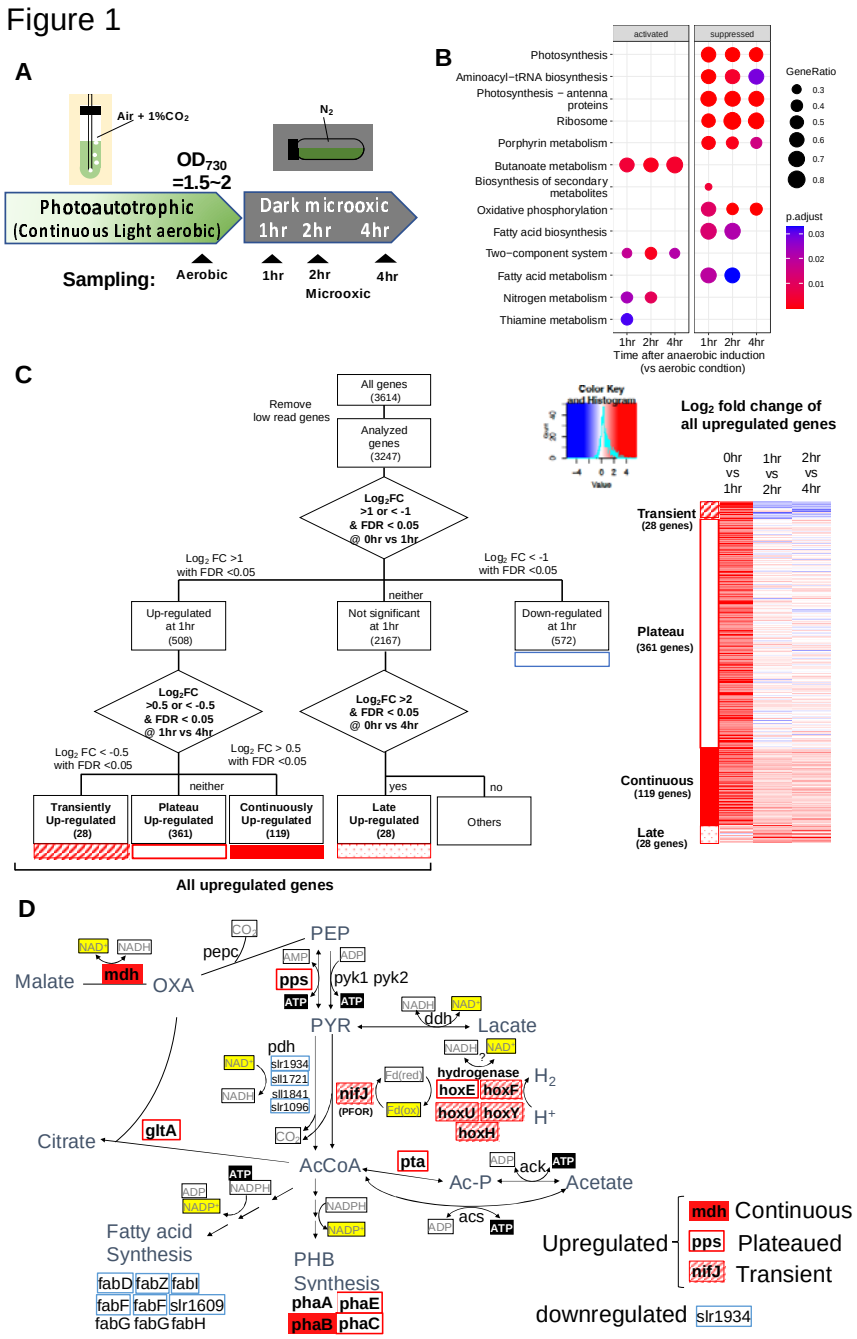

Figure 1

(A) Schematic diagram for the sampling of cells under aerobic and microoxic conditions. (B) Gene

set enrichment analysis on time-course transcriptome data. KEGG pathways enriched in upregulated or downregulated genes after 1-, 2-, and 4-h incubation under anaerobic conditions are shown. (C) (left) Schematic diagram showing the classification of genes according to the time-course transcriptome. Transient (striped square), Plateau (open square), Continuous (filled square), and Late (dotty square) are denoted as all upregulated genes. (right) Heatmap showing expression change in all upregulated genes over the time-course. Genes were clustered into subgroups and sorted by the gene name. (D) The classified genes were mapped to the central carbon metabolism, centered on pyruvate. PEP: phosphoenolpyruvate, PYR: pyruvate, AcCoA: acetyl CoA, Ac-P: acetyl phosphate, OXA: oxaloacetate, PHB: polyhydroxy butyrate.

Figure 2

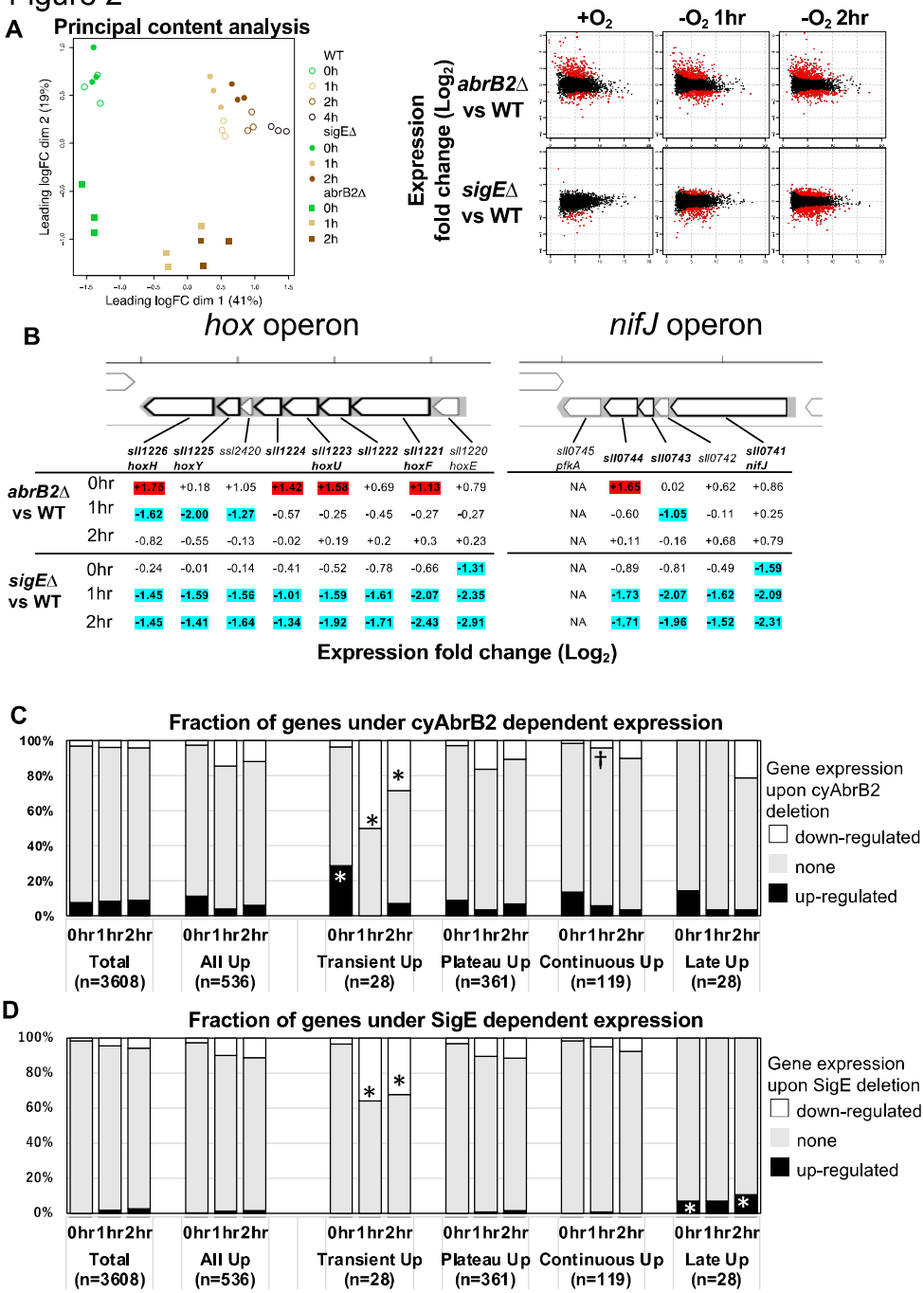

Figure 2

(A) (left) Primary component scatter plot showing the profiles of RNA-seq data. (right) MA plot

showing fold change (y axis) and average (x axis) of gene expression between wildtype and mutant strains at each timepoint. Red dots indicate defined DEGs ($|Log_2 FC| > 1$ with FDR < 0.05). (B) Log2 scaled expression fold change in genes in the *hox* and *nifJ* operons upon the deletion of CyAbrB2 and SigE under aerobic conditions (0 h), 1 hour after anoxic condition (1 hr), and 2 hour after anoxic condition (2 hr). DEGs are marked with sky blue (downregulated upon deletion) or red (upregulated upon deletion). (C and D) Fraction of upregulated and downregulated genes upon the deletion of (C) CyAbrB2 and (D) SigE at the timepoints of aerobic conditions (0 hr), 1 hour after anoxic condition (1 hr), and 2 hour after anoxic condition (2 hr). Genes are classified according to Figure 1C. Asterisk (*) and dagger (†) denote statistically significant enrichment and anti-enrichment compared with all upregulated genes tested by multiple comparisons of Fisher's exact test (FDR < 0.05).

Figure 3

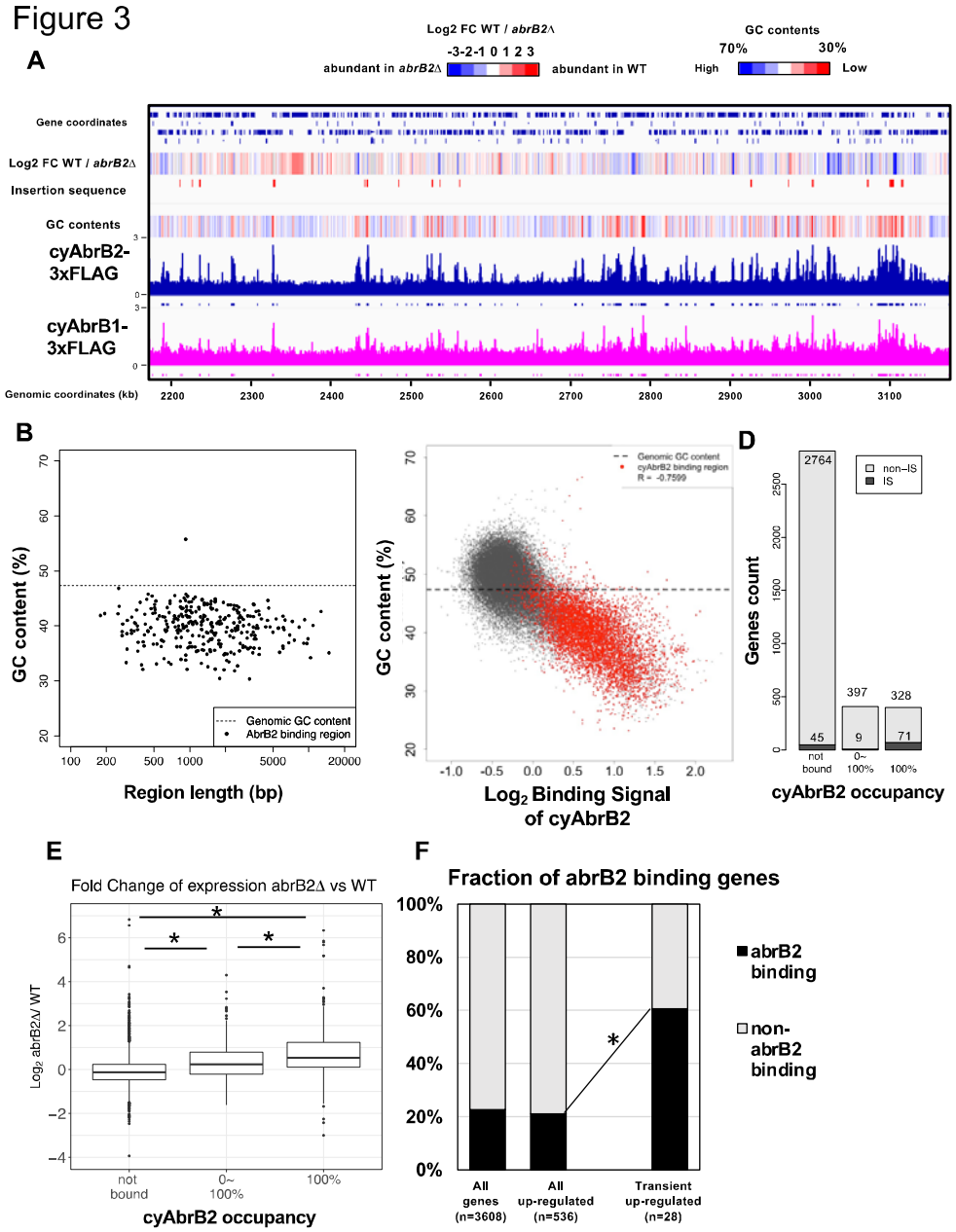

668

669 **Fi**

670

671

Figure 3 (continuing)

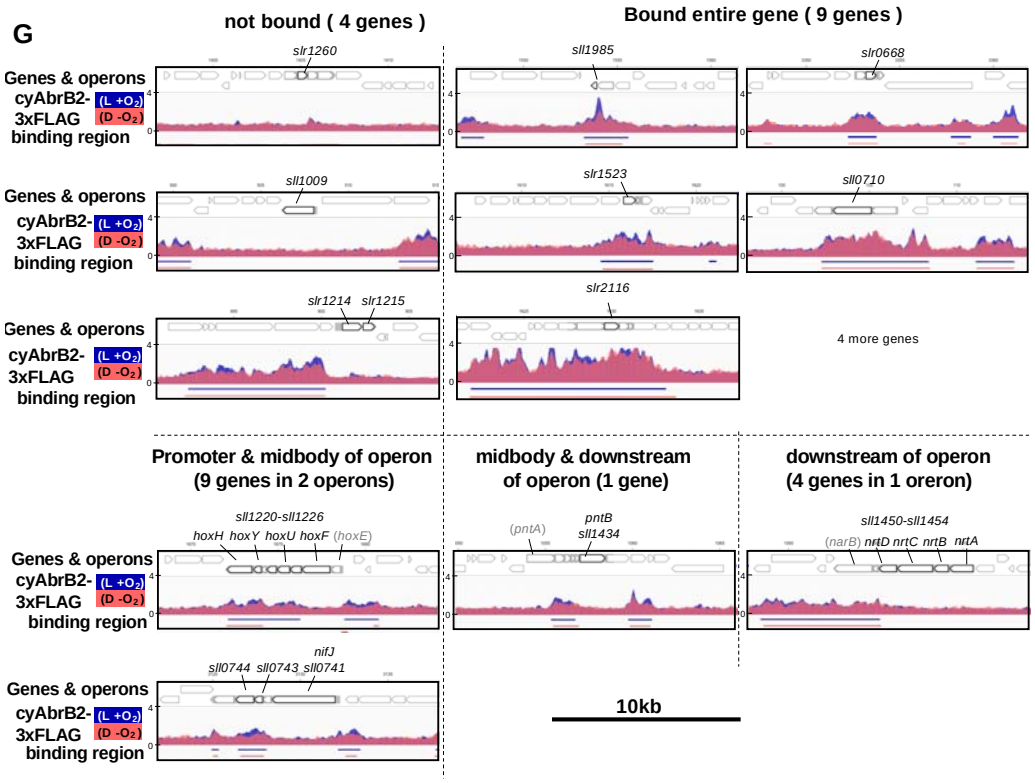

Figure 3

(A) Snapshot of ChIP-seq data for CyAbrB2 and CyAbrB1 under aerobic conditions. The heatmap in the second column indicates expression fold change upon CyAbrB2 deletion under aerobic conditions. Positive values (colored in red) indicate that the gene expression is higher in wildtype than in *cyabrB2*Δ, and negative values (colored in blue) indicate the opposite. The third column indicates the positions for the insertion elements. The heatmap in the fourth column indicates GC contents. High GC content are colored in blue and low GC contents are colored in blue.

(B) GC contents and region length of CyAbrB2 binding regions (black dots). The horizontal dotted

line indicates the genomic average of GC content.

(C) Scatter plot of GC content and binding signal of CyAbrB2. The x axis is the binding signal of CyAbrB2 in each 100 bp region, and the y axis indicates GC contents within 500 bp windows sliding every 100 base pairs.

(D) Histogram of genes showing the extent of occupancy (not bound, partially overlapped, or entirely overlapped) by the CyAbrB2 binding region. The gray bars indicate non-IS genes, and the count numbers of the non-IS genes are displayed on the gray bars. The black bars indicate the IS genes, and the count numbers of the IS genes are displayed on the black bars.

(E) Boxplot showing fold change in gene expression by CyAbrB2 deletion under aerobic conditions. Genes are classified according to the extent of occupancy by the CyAbrB2 binding region. Asterisk (*) denotes statistically significance tested by multiple comparisons of the Wilcoxon-rank test.

(F) Fraction of genes overlapped or non-overlapped with CyAbrB2 binding regions at the timepoints of aerobic conditions. Genes are classified according to Figure 1C. Asterisk (*) denotes statistically significant enrichment compared with all upregulated genes tested by multiple comparisons of Fisher's exact test.

(G) Distribution of CyAbrB2 around transiently upregulated genes. ChIP-seq data in aerobic (L + O_2) and dark microoxic (D − O_2) conditions are overlayed. Arrows with bold lines indicate transiently upregulated genes. Shaded arrows indicate operons whose data were obtained from a

previous study. The bars below the graph indicate the binding regions of each protein. The black bar top of the figure indicates a length of 10 kbp.

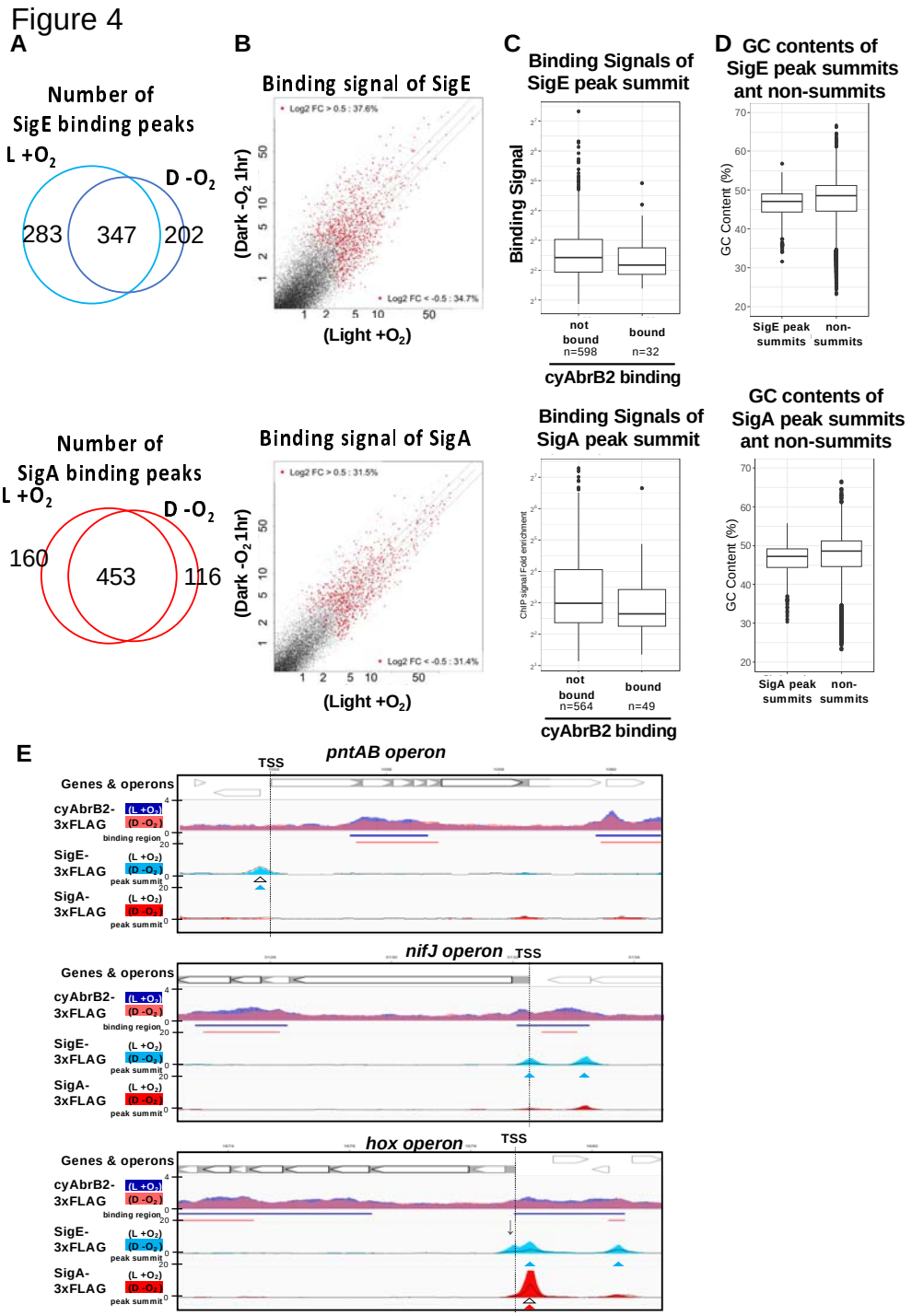

Figure 4

(A) Venn diagram showing the number of peaks of SigE and SigA in aerobic (L + O_2) and dark

microoxic (D − O_2) conditions. (B) Scatter plot showing changes in the binding signal of SigE and SigA by 1 hour cultivation under microoxic conditions. The binding signal of each 100 bp window is plotted. The binding signals are plotted in Figure 3E. (C) Distribution of ChIP enrichment signals of SigE and SigA peaks. The peaks were classified into two based on whether they overlapped with the CyAbrB2-binding region. (D) (E) Snapshots of ChIP-seq data for CyAabrB2, SigE, and SigA at the *nifJ* region (top) and *hox* region (bottom). ChIP-seq data for CyAbrB2, SigE, and SigA under aerobic and dark microoxic conditions are overlayed. ChIP-seq data of CyAbrB2 under aerobic and microoxic conditions are colored blue and pink, respectively. ChIP-seq data for SigE and SigA are shown in solid lines (aerobic conditions) and filled lines (microoxic conditions). The positions of TSSs were obtained from a previous study (Kopf et al., 2014) and indicated by vertical dotted lines. Open triangles indicate peak summits under aerobic conditions, and solid triangles indicate peak summits under microoxic conditions.

Figure 5

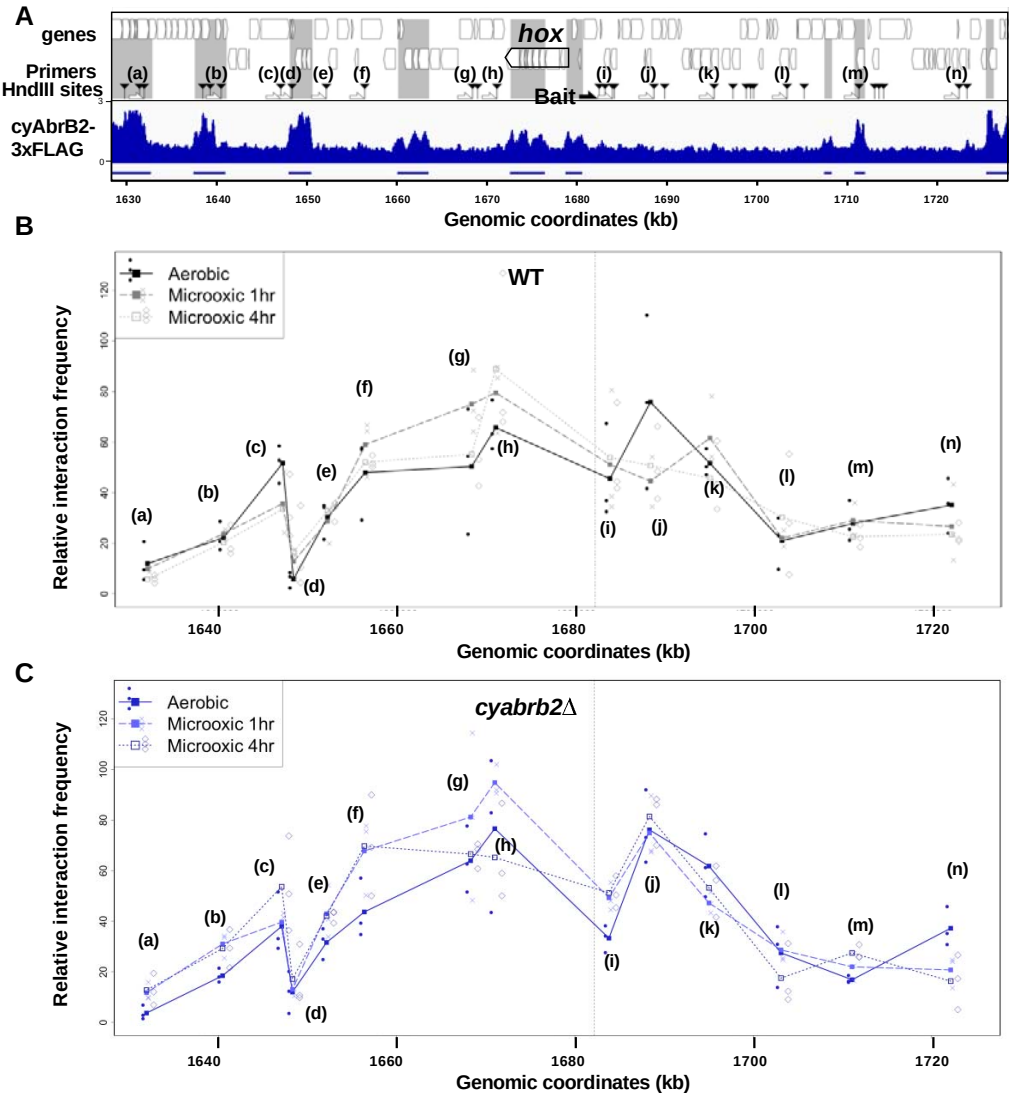

Figure3 (continuing)

Figure 5 (continued)

D

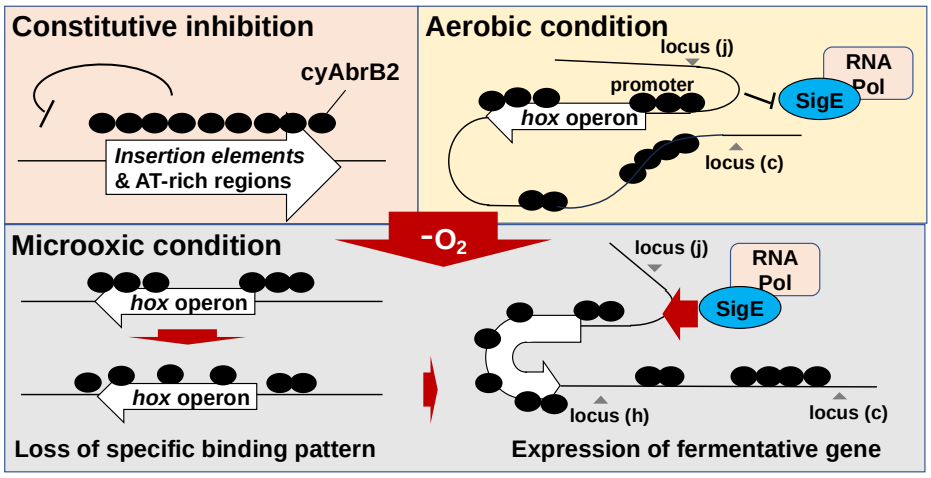

Figure 5

(A) Schimatic diagram of 3C analysis around *hox* operon.The black arrow shows localiton of the bait primer, and white arrows ((a) to (n)) incidicates loci where the interaction frecuency with bait were assayed. Black arrowheads indicate the position of HindIII sites. ChIP-seq data of cyAbrB2 in the aerobic condtion is displayed in bottom, and cyAbrB2 binding region are marked with shade. (B) and (C) The line plot showing the interaction frequency of each loci with *hox* framgent in the wildtype (B) and cysbrb2Δ (C) .The solid line, dashed line, and dotty line indicate data in the aerobic condtion, 1hr and 4hr cultivation of microoxic condtions, respectively. The line plots indidate the average of the interaction frequency over the random ligtion (n=3). Indivisual data are plotted (D) Schematic diagram of the dynamics of transcription factors governing fermentative gene expression.

Figure S1

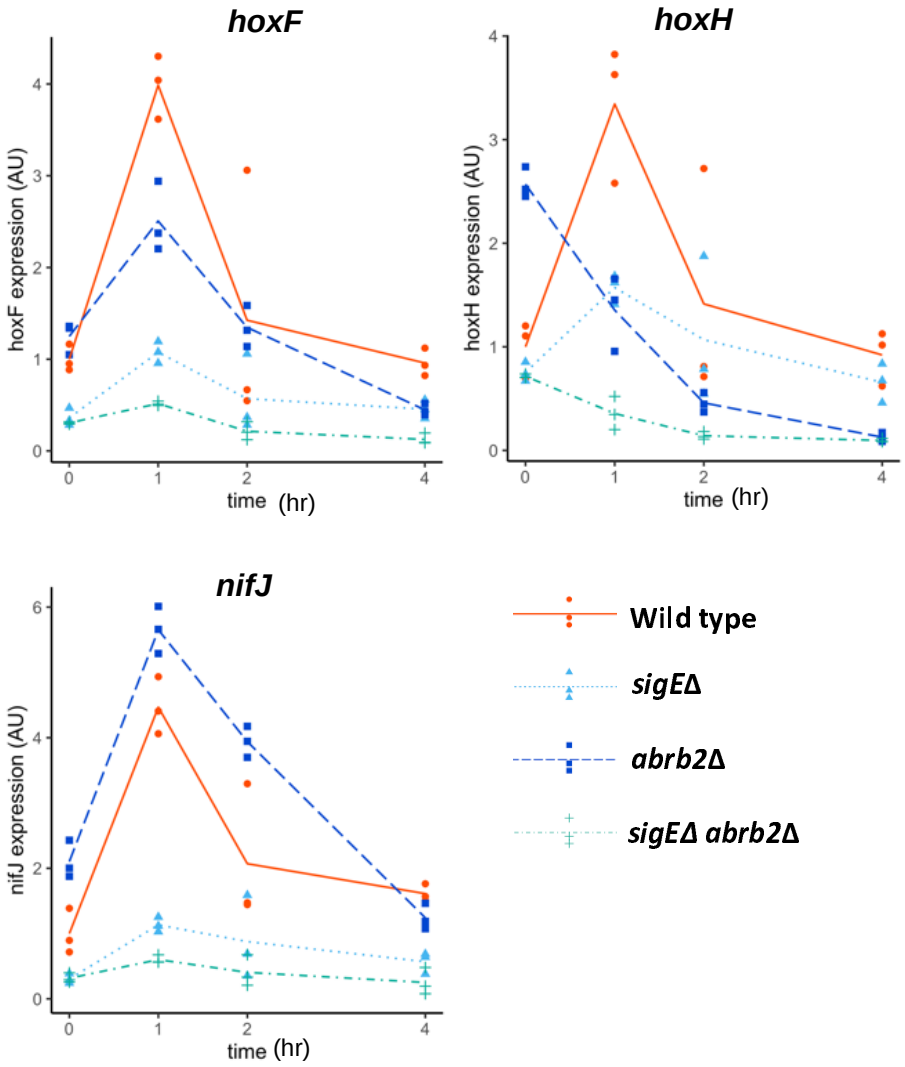

Figure S1

RT-qPCR validated the transiently upregulated genes classified by RNAseq. As the representative of the transiently upregulated genes, expression of *hoxF*, *hoxY* and *nifJ* were quantified by RT-qPCR. Transcripts extracted from wildtype (solid line), *sigE*Δ mutant (dotty line), *abrb2*Δ mutant (dashed line), and *sigE*Δ *abrb2*Δ double mutant (dot-dashed line) were assayed . The line represents the

743 mean of n=3, and individual data points are shown as dot plots.

Figure S2

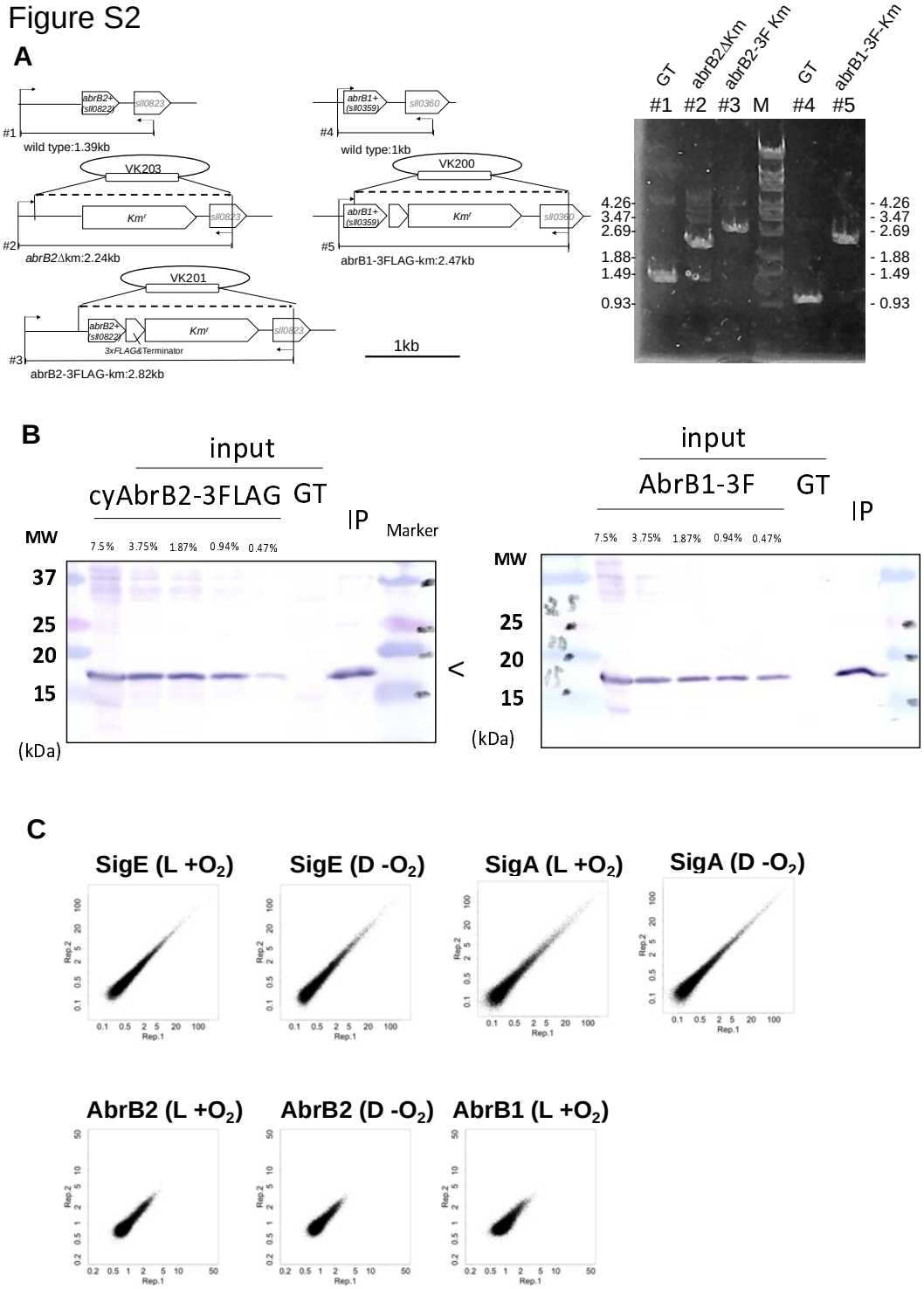

Figure S2 (continuing)

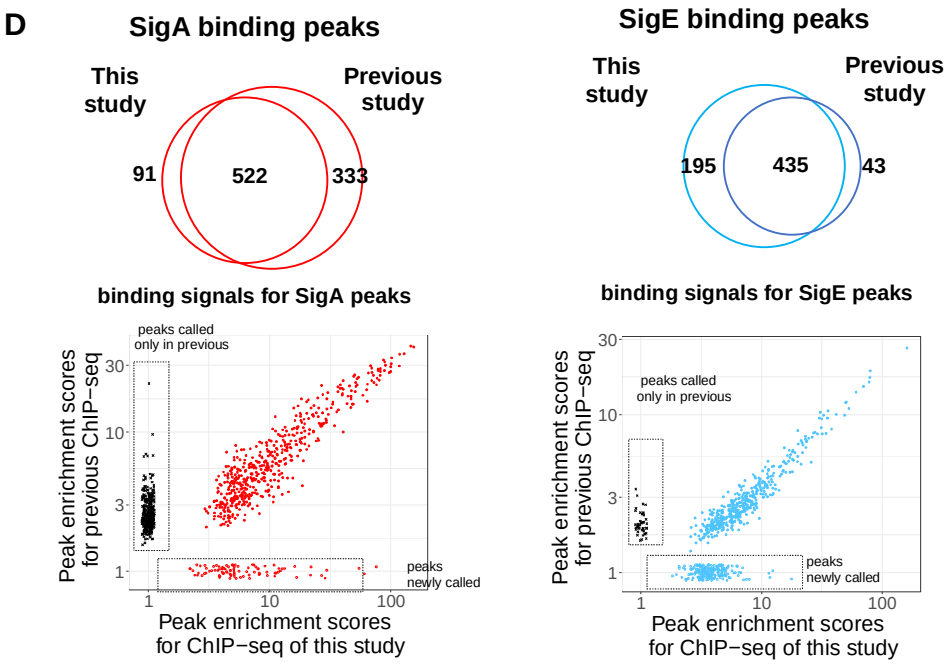

Figure S2

Validation of procedure for ChIP-seq of flag tagged cyAbrB2, SigE, and SigA.

(A) Confirmation of genomic deletion and the epitope tagging of abrB2 (#1-#3) and the epitope tagging of abrB1 (#4 and #5). (B) The immunoblot for inputs and immunoprecipitants of ChIP for cyAbrB2-FLAG and cyAbrB1-FLAG. Inputs equivalent to indicated portion of IP were loaded. (C)Scatter plots showing reproducibility of two replicates for ChIP-seq assay. ChIP-seq data of SigE, SigA, and cyAbrB2 in aerobic and microoxic conditions and ChIP-seq data of cyAbrB1 in the aerobic condition are shown. Dots indicates normalized IP read count / normalized input read count in each 100bp windows. X axis is value of replicate1 and Y axis is value of replicate 2. (D) Reproducibility of ChIP-seq data of SigA and SigE, compared with the previous study (Kariyazono and Osanai 2022). (top) Pie charts show overlapping of peaks called in this study and the previous

study. (bottom) Scatter plot comparing ChIP binding signals of SigA and SigE peaks commonly called in present and previous studies. Plots boxed by dashed line are peaks called only in present or previous study.

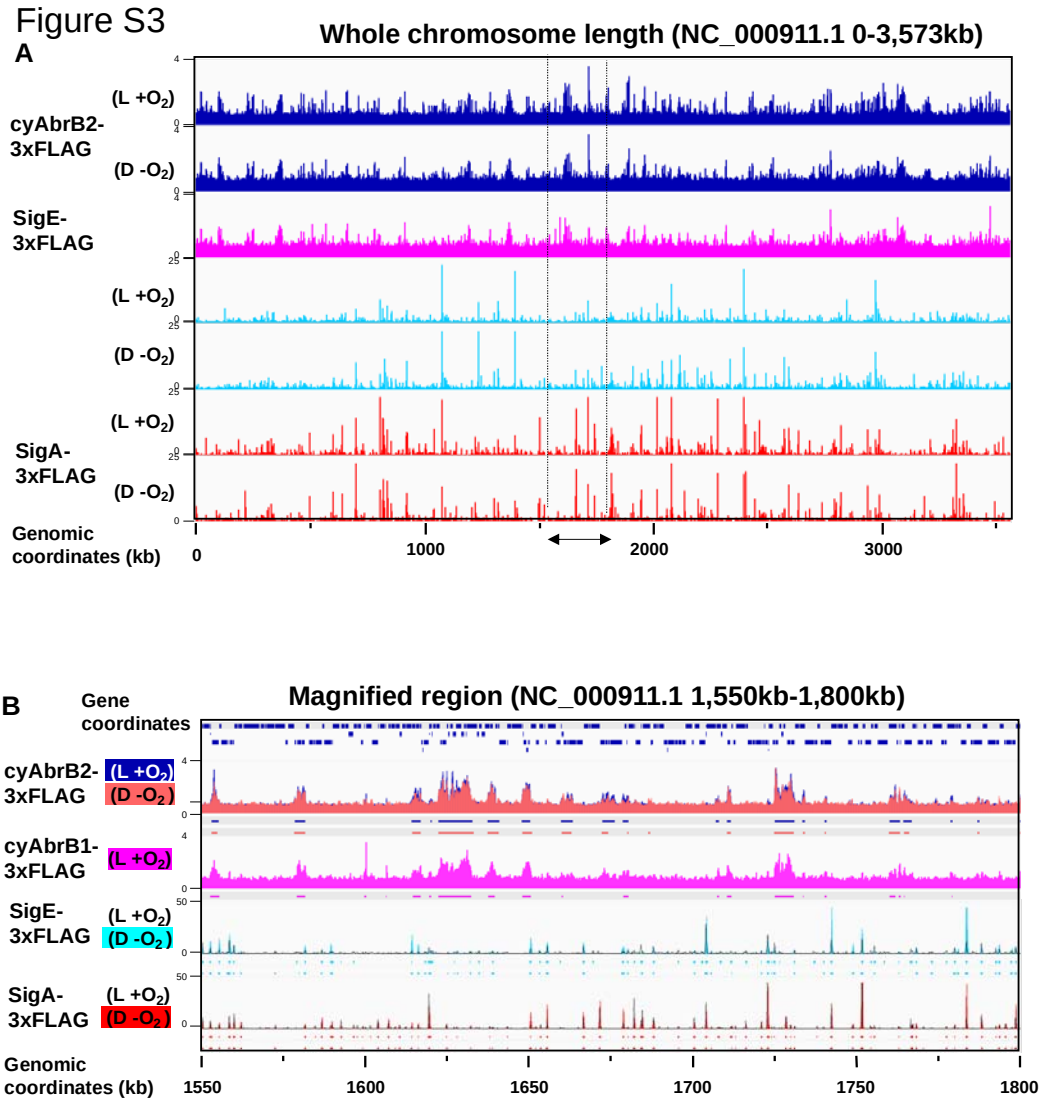

Figure S3

Overview for ChIp-seq of flag tagged cyAbrB2,cyAbrB1, SigE, and SigA. Y-axis indicates [normalized IP read count / normalized input read count at each 25bp window] and X- axis indicates chromosome position.

(A) Distribution of cyAbrB2, cyAbrB1, SigE, and SigA across the whole genome of *Synechocystis.* Data in aerobic (L +O_2) and dark microoxic (D -O_2) are displayed. (B) Magnified image for

chromosome position of 1,550kb-1,800kb. ChIP-seq data of cyAbrB2, cyAbrB1, SigE and SigA in aerobic and dark microoxic conditions are overlayed. Dots below graph indicates binding region of each protein calculated by peak caller.

Figure S4

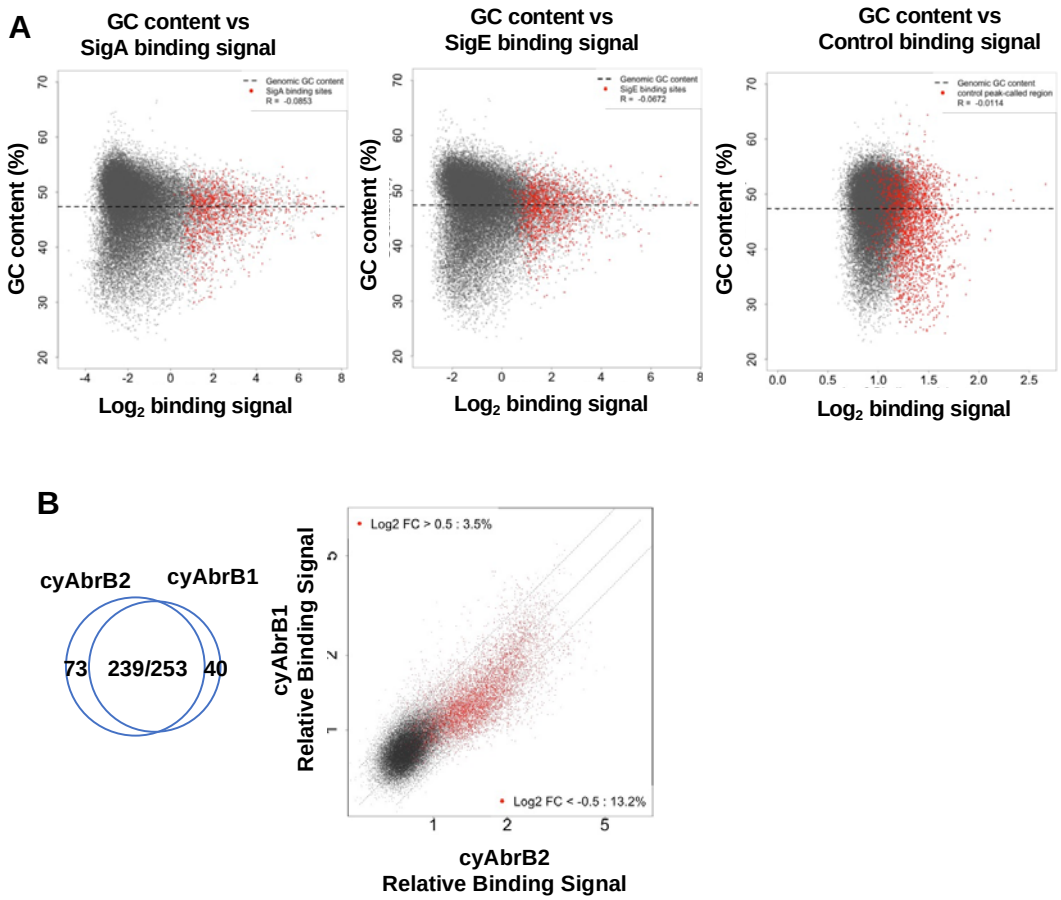

Figure S4

(A) Scatter plot showing GC contents in each 100bp vs binding signal of SigA, SigE, and control IP. Data are shown as in Figure 3C.

(B) Venn diagram showing overlap of binding region of cyAbrB1 and cyAbrB2 (left), and scatter plot showing ChIP binding signal of cyAbrB2 (y axis) and cyAbrB1(x axis) in the aerobic condition. data is plotted as in Figure 4E.

Figure S5

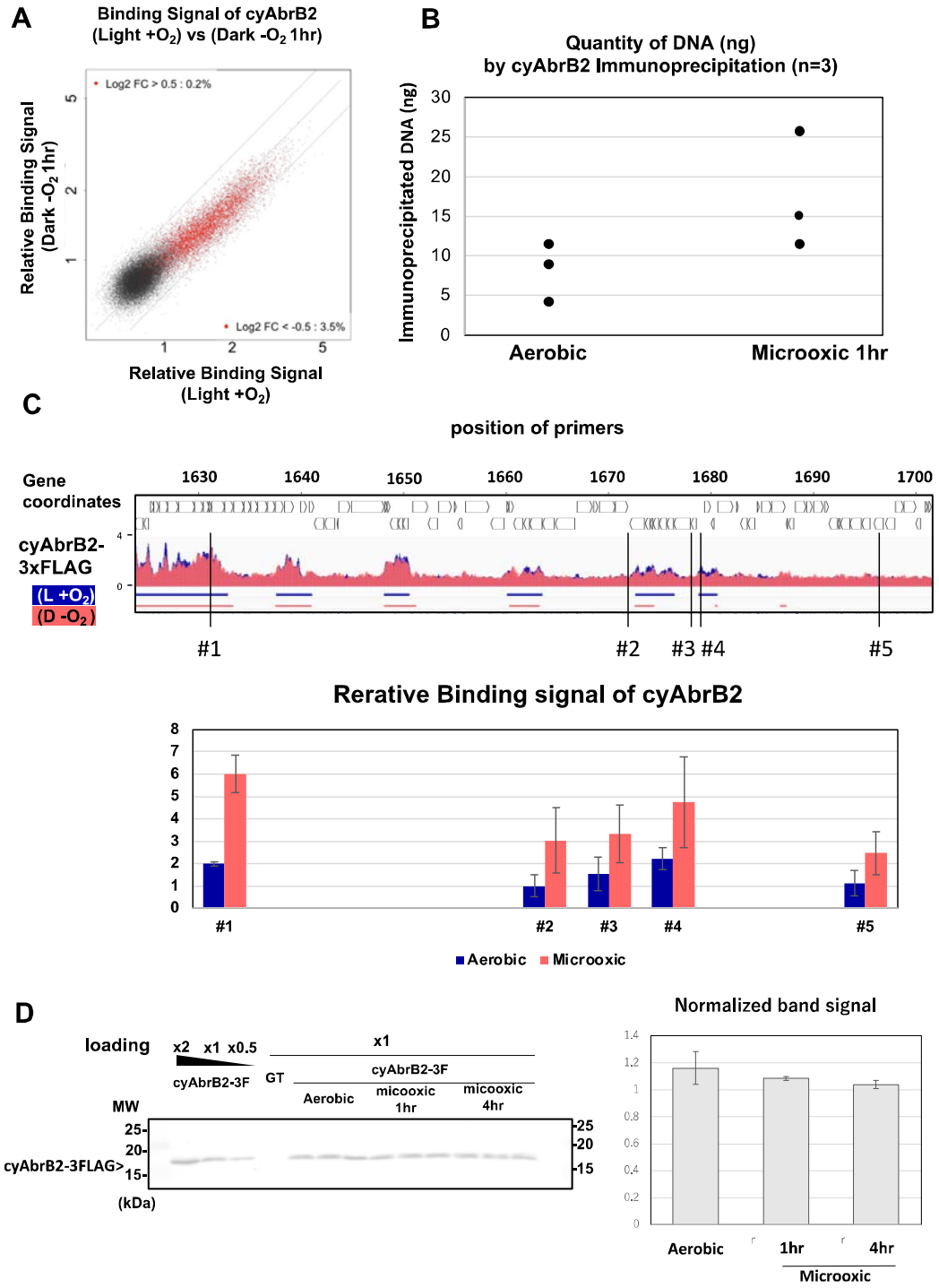

Figure S5(continuing)

Figure S5

(A) Scatter plot showing changes of binding signal by 1hr cultivation in the microoxic condition. Binding signal of each 100bp windows are plotted. Red dots are cyAbrB2 binding region in either aerobic or microoxic condition. The dotty lines indicate Log2 fold enrichment of 0.5, 0, -0.5 between aerobic and microoxic conditions. (B) Amount of precipitated DNA by cyAbrB2 ChIP. Three experiments were performed in the aerobic and microoxic conditions. (C) Quantification for ChIP of cyAbrB2 by qPCR. The position of primers and ChIP-seq data of cyAbrB2 are shown in top. (D) Western blot images of cyAbrB2-3FLAG. Proteins were extracted in the aerobic condition and 1hr and 4hr incubation under microoxic conditions. Total protein concentration of each sample was adjusted to 4mg/mL measured by BCA method. Quantification of cyAbrB2 from western blot image were performed by ImageJ (ver. 2.0.0-rc-65) and plotted in the right graph.

Figure S6

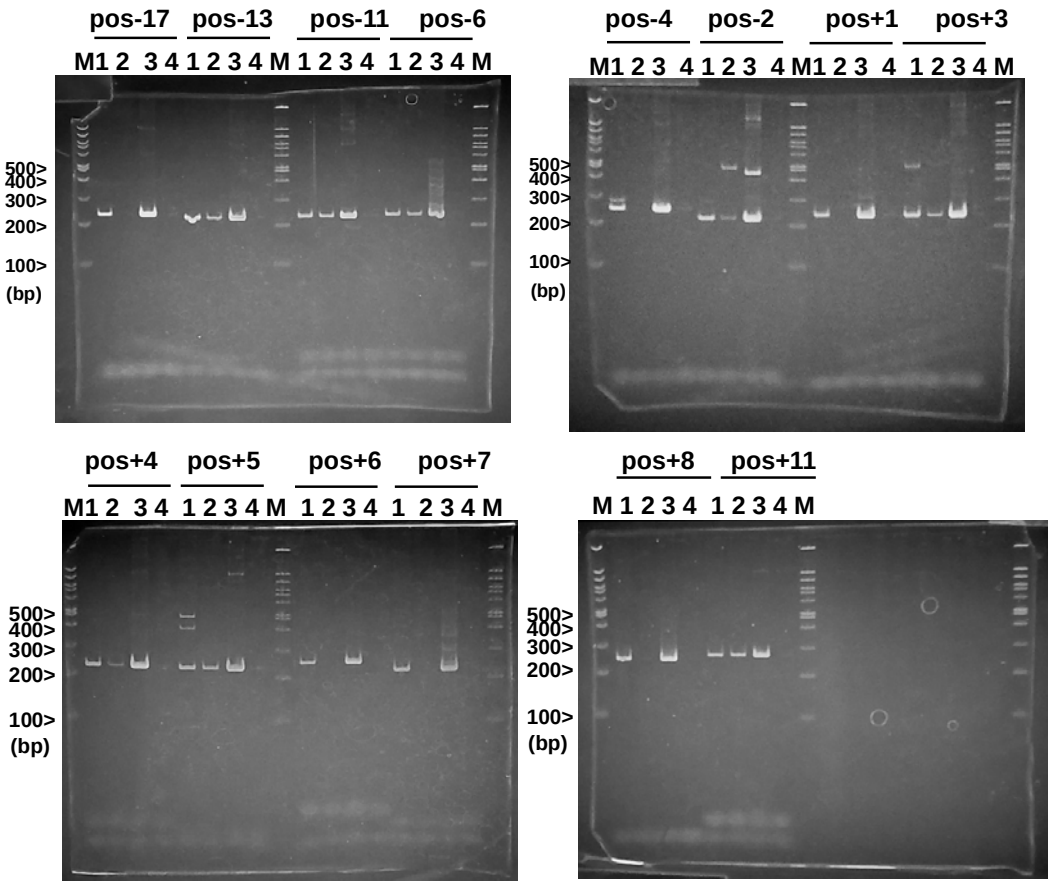

M:100bp ladder (DM2100 SMOBIO)
1 Calibration sample x500
2 Calibration sample x2500
3 3C sample x100
4 Unligated sample x100

GoTaq® Hot Start Program

95˚C 2min
95˚C 15sec | **x35**
60˚C 30sec
4˚C Hold

Figure S6

Validation of unidirectional primer sets for 3C assay shown in Figure 5. 3C sample in this assay is the mixture of all 3C samples assayed in Figure 5.

Figure S7

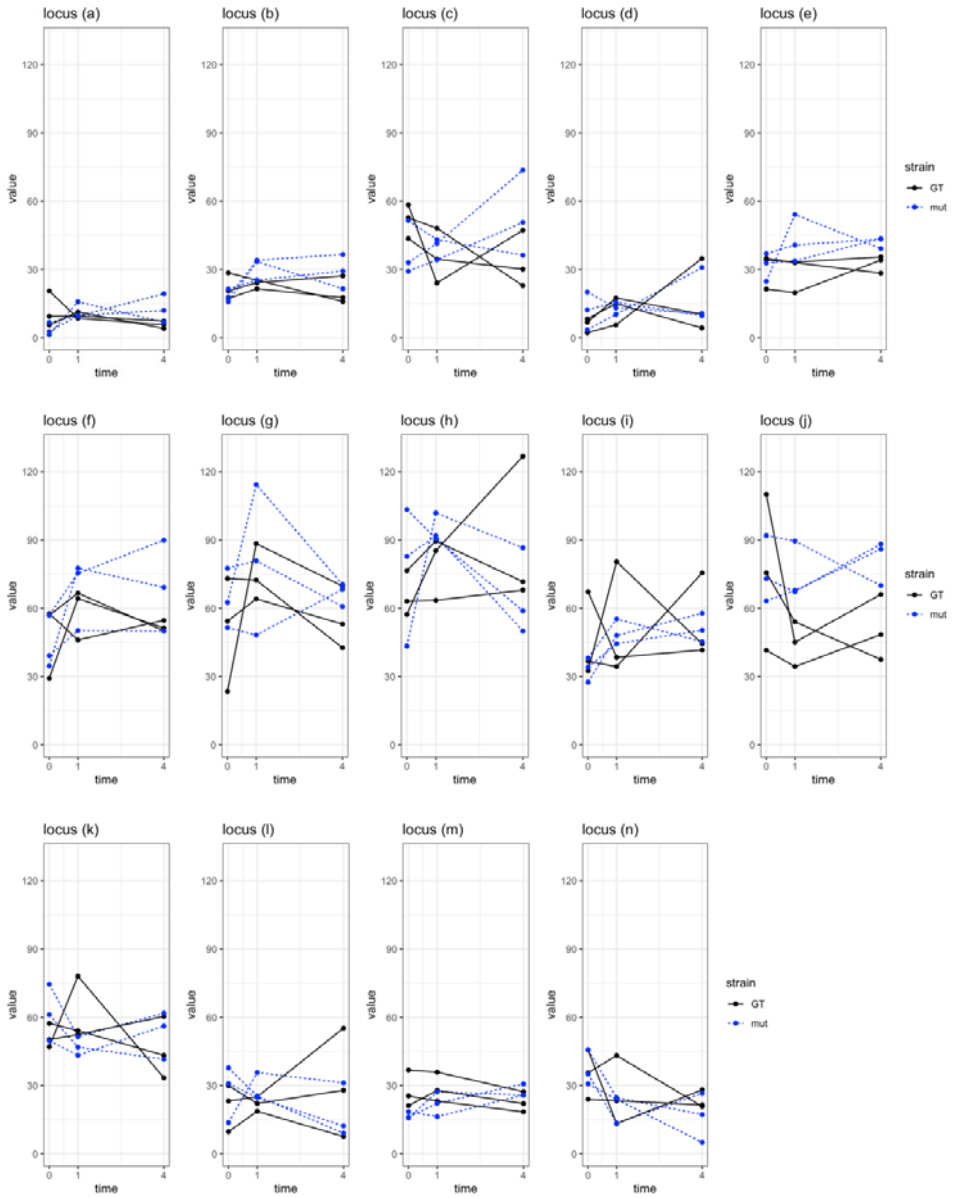

Figure S7

Re-plotting of Figure 5B and 5C with x-axis showing time (0,1,4 hr in microoxic conditions) and the y-axis showing the interaction frequency. Plots from the individual samples are connected by solid (Wildtype) or dotty (*cyabrb2*Δ) lines.

Table S1 List of strains used in this study

Strain ID	Host strain	genotype	Reference
GT			Williams, 1988
G50	GT	*sigE*Δkm	T. Osanai, et al,2005
KR93	GT	SigA-8His-km	(Kariyazono and Osanai 2022)
KR94	GT	SigA-3FLAG-km	(Kariyazono and Osanai 2022)
KR340	GT	*abrB2*ΔKmR	in this study
KR338	GT	AbrB(sll0359)-3xFLAG-Km	in this study
KR339	GT	AbrB2(sll0822)-3xFLAG-Km	in this study

Table S2 plasmids used in this study

Plasmid ID		backbone	
VK200	AbrB1-3F-km	pTA2 (Toyobo)	transformation for KR338
VK201	AbrB2-3F-km	pTA2 (Toyobo)	transformation for KR339
VK203	abrB2Δkm	pTA2 (Toyobo)	transformation for KR340

Table S3 oligonucleotides used in this study

Oligonucleotides ID		sequence
ChIP_slr2118_F1	Figure S5C #1	CATTTCAAGCGAGATAGCAG
ChIP_slr2118_R1	Figure S5C #2	TGGAAAGTGCCTGTTCAAAG
ChIP_ThoxH_F	Figure S5C #2	CATCACCGAGGGCATATCTAG
ChIP_ThoxH_R	Figure S5C #2	ACATAAGGCTATGGAAACC
ChIP_pHox_2F	Figure S5C #3	ACAGAGGATGGACAAATGTC
ChIP_pHox_2R	Figure S5C #3	TACCGCTTCGTCATTCTGCT
ChIP_pHox_up_2R	Figure S5C #4	TCGATTACTTCCCTTTAGTG

ChIP_pHox_up_2F	Figure S5C #4	CTTCGGCTCCATGTATTC
ChIP_sll0814_F	Figure S5C #5	GTTACTACCGCTATCTATCG
ChIP_sll0814_R	Figure S5C #5	ATGACGTAAACCGGCTCTGAC
3Chox_Hcommon	Figure 5	CGGTCCCTTTGGACGTAATC
3Chox_H01_pos_+1	Figure 5	GGGTTGGGCGCAACATTAAG
3Chox_H02_pos_+3	Figure 5	CAAAGCGATTTTGGCTGGTG
3Chox_H03_pos_+4	Figure 5	GATGTGGTGGAAGATACGGAC
3Chox_H04_pos_+5	Figure 5	GGAGCCACAGGGGAATTTAAC
3Chox_H05_pos_+6	Figure 5	GGTCAGATTTTATTGGTTGCATGG
3Chox_H06_pos_+7	Figure 5	TTGTCAATGTCAACCGCAAC
3Chox_H07_pos_+8	Figure 5	TTATTGCCCAATCTGGCGAC
3Chox_H08_pos_+11	Figure 5	AGGCAAGACAGATAAACCTTCTG
3Chox_H09_pos_-2	Figure 5	GGGGCATAGGGAGCAAACC
3Chox_H10_pos_-4	Figure 5	GGGGTAGTACCGGAAGTGG
3Chox_H11_pos_-6	Figure 5	TTGGGCTGATTCTTGCAATTC
3Chox_H12_pos_-11	Figure 5	AGCTTTTGTCTAACACCGTATCG
3Chox_H13_pos_-13	Figure 5	AAGCCATCCTTCAAAACCCG
3Chox_H14_pos_-17	Figure 5	GCCCCATCGGTGAGAAAAAG
qPCR_hoxF_F	Figure 5 (internal control)	GTCATCTGCAATGCTGACGAA
qPCR_hoxF_R	Figure 5 (internal control)	CCAACACACTGCGGTCCAT